SIAM J. Applied Dynamical Systems
Vol. 11, No. 1, pp. 416–446

A Saddle in a Corner—A Model of Collinear Triatomic Chemical Reactions*

L. Lerman† and V. Rom-Kedar‡

Abstract. A geometrical model which captures the main ingredients governing atom-diatom collinear chemical reactions is proposed. This model is neither near-integrable nor hyperbolic, yet it is amenable to analysis using a combination of the recently developed tools for studying systems with steep potentials and the study of the phase space structure near a center-saddle equilibrium. The nontrivial dependence of the reaction rates on parameters, initial conditions, and energy is thus qualitatively explained. Conditions under which the phase space transition state theory assumptions are satisfied and conditions under which they fail are derived.

Key words. Hamiltonian chaos, systems with impacts, transition state theory

AMS subject classifications. 70H07, 70H08, 70H09, 70H11, 70H12, 70H14, 37J45, 70F35, 80A50

DOI. 10.1137/110833890

1. Introduction.

The study of classical, semiclassical, and quantum chemical reactions on a molecular level has a rich history [1, 2, 3, 4, 5, 6, 7, 8, 9]. In these models, the full Hamiltonian is averaged over the fast motion of the electrons, where each electron is assumed to be fixed at a specific quantum energy level (the adiabatic approximation) [1, 2, 3]. Such computations produce effective potential energy surfaces (PESs) that govern the slow motion of the nuclei. The resulting Hamiltonians correspond to the *"Born–Oppenheimer"* approximation. Quasi-classical computations[1] that employ these Hamiltonians provide surprisingly good approximations to the quantum calculations, and hence classical models are extensively studied by chemists; see [1, 2, 3] and the references therein.

Dishearteningly, the resulting nuclei motion of even the most basic, classical "elementary" (bimolecular) reactions, which are "at the heart of chemistry" [3], is not well understood. Numerical simulations of the nuclei dynamics exhibit sensitive dependence of the trajectories on initial conditions and parameters. Moreover, one finds that macroscopic observables, like

*Received by the editors May 12, 2011; accepted for publication (in revised form) by T. Kaper December 24, 2011; published electronically March 20, 2012. This research was supported by RFBR (Russia) and MSTI (Israel) under grant 06-01-72023.

http://www.siam.org/journals/siads/11-1/83389.html

†Department of Differential Equations and Mathematical Analysis, The University of Nizhny Novgorod, Nizhny Novgorod, Russia (lermanl@mm.unn.ru). This author's research was partially supported by RFBR under grant 10-01-00429a, RFBR and the administration of the Nizhny Novgorod region under grant 11-01-97017 (regional-Povolzhye), the Ministry of Education and Science of the Russian Federation (contract NK-13P-13, P945), and the Russian Federation Government grant (contract 11.G34.31.0039).

‡The Estrin Family Chair of Computer Science and Applied Mathematics, The Weizmann Institute of Science, Rehovot 76100, Israel (vered.rom-kedar@weizmann.ac.il). This author's research was supported by the Israel Science Foundation (grant 273/07) and the Minerva Foundation.

[1]In these computations the atomic motion is found from the classical dynamics dictated by the PES. The quantization enters through choosing initial quantized ensembles (usually only in vibrational and rotational energies) and through binning of the product states to quantized energies.

reaction rates, have an intricate dependence on the parameters and energy; see, e.g., [1, 2, 3, 5, 8].

In contrast, the popular transition state theory provides an appealing intuitive view of this motion and leads to explicit formulae relating the microscopic nuclei kinetics to the macroscopic reaction rates. This theory assumes that the PES is separable to a one-dimensional potential ("along the reaction path") and a potential well in all the other modes of motion (the bath of oscillators). Hence, the reaction according to this theory is described by a product of a one degree of freedom (thus integrable) system and oscillators. This appealing phenomenological model is too simple: it does not describe the observed complex dependence of the nuclei motion on initial conditions and energy [1, 2, 3, 4, 5, 6, 7, 8, 9].

The next level of approximation, by which the nonoscillatory part of the potential is two-dimensional, is the subject of our paper. Here, the translational and vibrational energies of the atom and diatom are coupled to each other yet are separable from all the other modes of motion (e.g., of those associated with the bending and the rotational energies). Such a decoupling occurs, for example, when the initial configuration is collinear and the angular momentum is zero [4, 5]. This separability assumption is widely used in theoretical investigations of chemical reactions [1, 2, 3, 4, 5, 6, 7, 8, 9]. Indeed, the first examinations of the principles underlying the transition state theory were conducted by investigating such models [4, 5].

Employing such a restrictive reduction[2] still leaves us with a two degrees of freedom system which may admit chaotic behavior (in contrast with the transition state theory reduction which leaves us with integrable dynamics). One source for such complicated behavior is associated with the existence of a reaction barrier—a saddle point of the PES.[3] The existence of such a barrier is the main ingredient needed for relating the classical transition state theory to the analysis of the phase space structure of two degrees of freedom systems [5, 12, 13, 14, 15, 16]. Normal form analysis of the local phase space structure near the PES bottlenecks (local unstable extremal points of the PES) relates these two approaches and leads to accurate calculations of the minimal flux through them [12, 10, 11]. The local picture near the bottlenecks does not reveal the complexity of the motion. This complexity is revealed only when the global structure of the reaction tubes—the phase space regions that pass through the bottlenecks—is calculated [5, 6, 12, 13, 14, 17, 18, 19].

Previous works on the global features of these tubes have either employed near-integrable techniques [8, 20, 14, 21] or numerical integrations [5, 6, 12, 13, 14, 17, 18, 19]. In these works it is demonstrated that the structure of the stable and unstable manifolds of unstable periodic orbits (the periodic orbits dividing surfaces (PODSs) [5] or, similarly, the stable and unstable manifolds of the normally hyperbolic invariant manifolds (NHIMs) [12, 18]) determines the reaction rates. In particular, when these asymptotic surfaces intersect each other the reaction rates depend on both the intersection pattern and the local flux near the saddles. In such cases the predictions of the transition state theory (and its local minimal flux variants) must be modified. These insights are employed to study numerically the asymptotic surfaces to

[2]By which the bath of oscillators is considered to be separable from the reaction dynamics.

[3]Some reactions have potentials that also admit stable triatomic states (indirect reactions), many reactions have a single steady unstable triatomic configuration (direct reactions), and in some exceptional cases there are no steady triatomic configurations at all [5, 3]. Most recently, models with rank-k saddles have been considered as well [10, 11].

NHIMs of high-dimensional problems [12, 17].

Here we introduce a new geometrical model for the two-dimensional PES. The PES in the reaction region is approximated by a sum of a quadratic form with a saddle point and a smooth potential which is close to zero within a corner region and increases sharply at the corners' boundaries (see Figures 1(b) and 2). We analyze this model by combining the theory of smooth Hamiltonians with impacts [22, 23, 24, 25], the recent generalization of [26, 27] to the impact case [28], and the theory of homoclinic loops to a saddle-center [29, 30, 31]. The analysis provides qualitative understanding regarding the global structure of the dividing surfaces in reactions with one rank-1 saddle point. Indeed, we identify a basic mechanism which explains why and when the dividing surfaces of the periodic orbits that have energies slightly above the barrier energy are especially complicated or especially simple (namely, they do not intersect each other). Moreover, we provide a mechanism for the emergence of stable triatomic cyclic motion. The applicability of these geometrical insights to more accurate models of the PES and to higher-dimensional settings (e.g., when the two degrees of freedom dynamics are weakly coupled to a bath of oscillators) is under current study.

The paper is ordered as follows. In section 2 we recall that mass-scaled Jacobi coordinates bring the collinear triatomic reaction's Hamiltonian to a two degrees of freedom Hamiltonian in the standard mechanical form. In section 3 we introduce the geometrical potential function, and in section 4 we provide some basic observations regarding its properties and its relation to other potentials. In section 5 we analyze the dynamics in this model under specific geometrical conditions, proving that both chaotic and stable periodic triatomic motions emerge. In section 6 we show that complicated dynamics appear at some parameter ranges and simple dynamics at others. In section 7 we discuss the relation of these results to transition state theory and propose some possible extensions.

2. Collinear atom-diatom reactions. Some of the geometrical characteristics of the PES describing collinear triatomic reactions may be inferred from general considerations that are common to all such reactions. These characteristics, as described next, motivate our construction of the simplified geometrical model for the PES.

Consider the triatomic reaction $A+BC \to AB+C$. Namely, here we always consider the atom-diatom case. We denote this reaction by the standard shorthand notation $AB+C$. An effective Hamiltonian for the molecular interaction is of the form

$$H(r,p) = \sum_{i\in\{A,B,C\}} \frac{1}{M_i}\frac{p_i^2}{2} + V(r),$$

where $r = (r_A, r_B, r_C)$ denotes the positions of the atoms A, B, C in a given inertial frame and $\{M_i\}_{i\in\{A,B,C\}}$ denote the masses of the atoms. Under standard conditions V depends only on the relative positions of these atoms. This nine degrees of freedom system simplifies when collinearity is assumed [4, 5]. This assumption implies that the relative positions may be expressed in terms of two scalars $r_1 = (r_A - r_B)\cdot\widehat{e}$, $r_2 = (r_B - r_C)\cdot\widehat{e}$, where $\widehat{e}$ is a unit vector aligned with the molecules, namely $V(r) = V(r_1, r_2)$. Moreover, since at small distances the atoms are strongly repelling, V becomes large along the rays $r_i = 0$; see Figure 1(a). The kinetic energy term in these new coordinates is nondiagonal and has a mass-dependent quadratic form. A mass-weighted coordinate system (the Jacobi coordinates; see

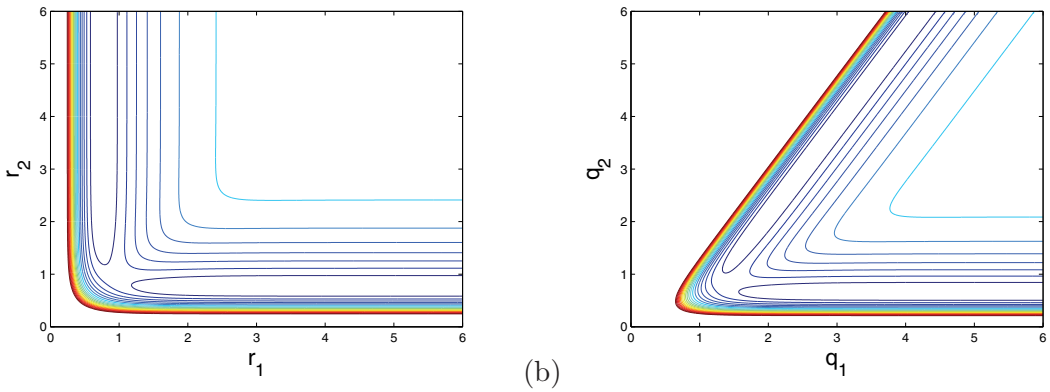

(a) (b)

Figure 1. *Contour lines of the effective potential for the $H_2 + H$ reaction in the* (a) *relative positions coordinates $V(r_1, r_2)$ and* (b) *mass scaled coordinates $V_r(q_1, q_2)$. The allowed region of motion lies within the dense contour lines (red lines) that correspond to the strong diatomic repulsion at small distances. In the (r_1, r_2) plane this region is essentially the positive quadrant, whereas in the (q_1, q_2) plane it is confined to a β-wedge/corner: a two-dimensional wedge with a corner angle $\beta = 60°$. The appearance of a single saddle point in the corner region is apparent. The plotted potential is of the LEPS form; see* [1, 2, 3] *and the references therein. Notably, the β-wedge feature always appears in the mass scaled coordinates, independent of the exact form of the potential.*

[2] for formulation and references) brings the system to the standard mechanical Hamiltonian form of a unit mass particle moving in the potential field $V_r(q_1, q_2)$:

$$H(q_i, p_i) = \frac{p_1^2}{2} + \frac{p_2^2}{2} + V_r(q_1, q_2). \tag{2.1}$$

Here, (q_1, q_2) are the reaction coordinates

$$q_1(r_1, r_2) = \hat{a}\, r_1 + \hat{b}\, r_2 \cos\beta, \quad q_2(r_2) = \hat{b}\, r_2 \sin\beta, \tag{2.2}$$

the scaling coefficients $\hat{a}, \hat{b}$ depend only on the mass of the atoms

$$\hat{a} = \sqrt{\frac{M_A(M_B + M_C)}{M_A + M_B + M_C}}, \quad \hat{b} = \sqrt{\frac{M_C(M_B + M_A)}{M_A + M_B + M_C}}, \tag{2.3}$$

and the mass-dependent "skew-angle" β is defined by

$$\beta = \arccos \sqrt{\frac{M_A M_C}{(M_A + M_B)(M_B + M_C)}}. \tag{2.4}$$

For the $H_2 + H$ reaction, $\beta = 60°$ (see Figure 1(b)); for heavy-light-heavy interactions, β is small (e.g., for $IH + I$, one finds $\beta = 7°$), whereas light-heavy-light interactions lead to $\beta \approx 90°$ (see [7, 5, 6, 2] for the corresponding figures and the references therein).

The short range repulsion of the atoms implies that the motion in the configuration space is confined by the rays $r_1 = 0$, $r_2 > 0$ (namely, $q_2 = q_1 \tan\beta$, $q_2 > 0$) and $r_2 = 0$, $r_1 > 0$ (namely, $q_2 = 0$, $q_1 > 0$). This region, a two-dimensional wedge in the (q_1, q_2) plane, is hereafter called

the corner region or the β-wedge; see Figure 1(b). The dynamics within the β-wedge depend on the particular form of the potential $V_r(q_1, q_2)$. We will mostly be considering potentials that have a single extremal point which is a saddle.

In the scaled coordinates, chemical reactions are represented by trajectories of the Hamiltonian (2.1). Reactant states (BC molecules and far away A atoms) correspond to configurations with a large q_1 and bounded q_2. We thus say that such configurations belong to the reactant channel. Similarly, product states (AB molecules and far away C atoms) correspond to configurations in the product channel with bounded $(q_1 \tan\beta - q_2)$ and large q_1, q_2. In the reactant (product) channel the potential is well approximated by a one-dimensional BC (AB) diatomic potential. The corner region, where both q_1 and q_2 are bounded and where all the potential saddle points are located, is called the reaction region. In symmetric cases with a single saddle point the saddle point is located on the bisector—the potential symmetry line. In nonsymmetric cases, the barrier location is called "early" (respectively, "late") if it is closer to the reactant (respectively, product) channel.

3. The geometrical potential function. The above description of the geometrical properties of the potential $V_r(q_1, q_2)$ is independent of the details of the reaction. Below, we propose a specific form for a potential $V_r(q_1, q_2)$ with parameters that have a transparent geometrical meaning. This potential may be viewed as a local geometrical approximation in the interaction zone to any other potential surface. The advantage of using this new formulation becomes apparent: It allows for rigorous analysis of the model and for qualitative understanding of the dynamics.

Consider Hamiltonians with geometrical potentials of the form

$$H(q, p; a, b, c, \varepsilon) = \frac{p^2}{2} + aV_a(q) + bV_b(q, \varepsilon) + cV_{farfield}(q). \tag{3.1}$$

Here $H_b = H(q, p; b, a = c = 0)$ is a billiard-like system limiting to a billiard in a β-wedge (see more details below). $H_{int} = H(q, p; a,\ b = c = 0)$ is an integrable system where the potential $V_a(q)$ has a single saddle point in the corner region (we will soon fix $V_a(q)$ to be a quadratic potential and remark on the effects of higher order terms when applicable). The far-field potential $cV_{farfield}(q)$ and its derivatives are small in the reaction region (yet are large away from the corner region). All together, $aV_a(q)$ corresponds to the normal form of the potential near the saddle point, $bV_b(q, \varepsilon)$ corresponds to the diatomic repulsion terms, and $cV_{farfield}(q)$ handles the remainder terms near the saddle and the reactant and product channels away from the corner region.

By billiard-like system we mean that the potential $V_b(q, \varepsilon)$ is a steep potential [32]: the level set of this potential at, say, $V_b = 1/2$ limits, as $\varepsilon \to 0$, to some billiard-like domain and $V_b(q, \varepsilon) \to 0$ for all q in the interior of this domain (see [27] for a precise definition and (3.4), (3.5) for examples). Here, the β-wedge is the billiard domain. For example, in Figure 1(b), the red level curves are identified with the level curves of $V_b(q, \varepsilon)$. For small a values (or, equivalently, at energy levels that are much larger than a), the smooth part of the potential at the corner region may be neglected and the motion in the β-wedge is billiard-like [26, 27].

For nonnegligible[4] a, for sufficiently small (ε, c), at a fixed positive energy level, the system

[4]Yet bounded, so that along the corner boundaries the diatomic repulsion dominates.

$H_\varepsilon = H(q,p;a,b,c,\varepsilon)$ has trajectories that closely follow the smooth integrable dynamics H_{int} until they reach the walls defined by $V_b(q,\varepsilon)$, reflect according to the billiard law, and continue with the smooth dynamics. Indeed, in the limit $\varepsilon \to 0$, the motion is described by a Hamiltonian system with impacts [22, 23, 24, 25]. Here, we study the dynamics of such impact systems when their smooth integrable part (H_{int}) has invariant hyperbolic subsets (here, Lyapunov periodic orbits near a saddle-center [33, 29, 30]). We prove that for a range of parameter values the reflections of the stable and unstable manifolds of this set from the billiards' boundaries give rise to complicated homoclinic behavior (Theorem 5.2) and to stable, recurrent triatomic states (Theorem 5.5). We also show that at a different range of parameter values the manifolds reflect to infinity via the reactant and product channels and no recurrent motion near the saddle is possible (Theorem 6.1 and Conjecture 6.5). For this latter range of parameters, transition state theory is expected to be valid.

Finally, the results established for the limiting impact flow at $\varepsilon = c = 0$ are shown to be valid at small ε, c. The persistence for small c values follows, as usual, from the robust character of these results under smooth perturbations. The persistence for small ε follows from the recent extension of [27] to smooth Hamiltonians that limit to impact systems [28].

3.1. The simplest form of the geometrical model. The assumption that the potential has a single saddle point in the corner region implies that the potential aV_a of (3.1) is of the form

$$aV_a(q) = \frac{1}{2}(q-q_s)^T A(q-q_s) + O((q-q_s)^3), \tag{3.2}$$

where A is a symmetric 2×2 matrix ($A^T = A$) with eigenvalues $(\omega^2, -\lambda^2)$. Additionally, since the potential saddle point $q_s = (q_{1,s}, q_{2,s})$ is assumed to be located within the corner region, it satisfies $q_{1,s} > 0$, $q_{2,s} < q_{1,s}\tan\beta$. Consequently (see section 4), the Hamiltonian flow has a saddle-center equilibrium at $P = (q,p) = (q_s, 0)$.

Replacing $aV_a(q)$ in (3.1) by its quadratic approximation we obtain the simplest form of the geometrical model:

$$H(q,p;b,c,\varepsilon) = \frac{p^2}{2} + \frac{1}{2}(q-q_s)^T A(q-q_s) + bV_b(q;\varepsilon) + cV_{farfield}(q). \tag{3.3}$$

Recall that the bV_b term corresponds to a billiard-like potential in the corner; namely, it satisfies conditions I–IV of [27]. We may, for example, consider here either an exponential potential (as in the repulsion associated with a Morse potential) or a power-law potential (as in the Pauli repulsion term of a Lennard-Jones interaction):

$$bV_b(q,\varepsilon) = bV_{exp}(q,\varepsilon) = b\exp(-q_2/\varepsilon) + b\exp((q_2 - q_1\tan\beta)/\varepsilon) \tag{3.4}$$

or

$$bV_b(q,\varepsilon) = bV_{pow}(q,\varepsilon/b) = \frac{\varepsilon}{q_2^k} + \frac{\varepsilon}{(q_1\tan\beta - q_2)^k}, \quad k \in \mathbb{Z}^+. \tag{3.5}$$

We study (3.3) in the small c regime; namely, we assume that the far-field term is small. We expect this approximation to be valid only in the reaction region. We thus study the

dynamics in a bounded corner region of the configuration space. The simplest model provides adequate approximation to (3.1) in this bounded region if the far-field potential and all its derivatives are small there and, additionally, $aV_a(q)$ is well approximated by its quadratic approximation. This latter part of the assumption may be relaxed in the future by including higher order terms of the normal form near the saddle-center point of the Hamiltonian.

The motion for $a, b \neq 0$ is found by analyzing first the singular impact limit (i.e., when $\varepsilon \to +0$), hereafter called the limit system. Then, the recent persistence results of [28] (generalizing [26, 27]) and standard perturbation theory allow us to establish that similar behavior persists for sufficiently small ε and c.

4. The phase space structure of the limit system and its dependence on parameters. In the limit $\varepsilon \to +0$ the behavior of (3.3) in the interior of the corner region is governed by the linear integrable system corresponding to the quadratic Hamiltonian. The limit system is defined as this smooth integrable motion inside the corner together with reflections from the corners' boundaries.

In section 4.1 we recall the integrable phase space structure of the quadratic Hamiltonian in the saddle-center case. In section 4.2 we recall the reflection law from the corners' boundaries. In section 4.3 we explain how the parameters of the simplest geometrical model (3.3) may be extracted from a general PES and motivate our choice of particular ranges of geometrical parameter values in sections 5–6.

4.1. The integrable structure near the saddle-center. Below, we first rotate the (q, p) coordinate system so that the quadratic Hamiltonian in (3.3) becomes separable (more generally, one brings the integrable part of (3.1) to its normal form near the saddle-center point). We then define the corner region in the rotated coordinate system (u, v); see Figure 2. We show that in the rotated system the projections of the stable and unstable manifolds of the saddle-center fixed point and of the nearby periodic orbits are easily found. We end this subsection by defining two constants of motion and identifying reacting and nonreacting trajectories near the saddle-center point in terms of the values of these constants of motion.

Denote the normalized eigenvector of A which corresponds to ω^2 (respectively, $(-\lambda^2)$) by U_1 (respectively, U_2). Recall that $U_1 \perp U_2$. A small computation shows that the eigenvalues of the saddle-center point of the Hamiltonian flow, $P = (q_s, 0)$, are $\pm i\omega, \pm\lambda$. The Hamiltonian flow has a two-dimensional real invariant subspace E^c (center plane) corresponding to the eigenvalues $\pm i\omega$: $E^c = \{(\widehat{q}, \widehat{p}) | (\widehat{q}, \widehat{p}) = (rU_1, sU_1),\ r, s \in \mathbb{R}\}$. The center plane projection onto the configuration space is one-dimensional, along the eigenvector[5] U_1. Similarly, the Hamiltonian stable and unstable subspaces corresponding to the real eigenvalues $\pm\lambda$ are expressed in terms of the matrix eigenvector U_2: $E^u = \{(\widehat{q}, \widehat{p}) | (\widehat{q}, \widehat{p}) = r(U_2, \lambda U_2),\ r \in \mathbb{R}\}$, $E^s = \{(\widehat{q}, \widehat{p}) | (\widehat{q}, \widehat{p}) = r(U_2, -\lambda U_2),\ r \in \mathbb{R}\}$. Thus, the projection of both the stable and unstable subspaces onto the configuration space is along U_2—the eigenvector of A corresponding to the negative eigenvalue $(-\lambda^2)$. The eigenvectors directions should not be confused[6] with

[5] If higher order terms of the normal form are included in aV_a, these statements apply to the tangent planes of the corresponding manifolds.

[6] These simple observations are the source of much confusion, as we wrongly tend to confuse the level sets of V_a in the configuration space q with the phase space plots in the space spanned by the stable and unstable directions (see Figures 2 and 3).

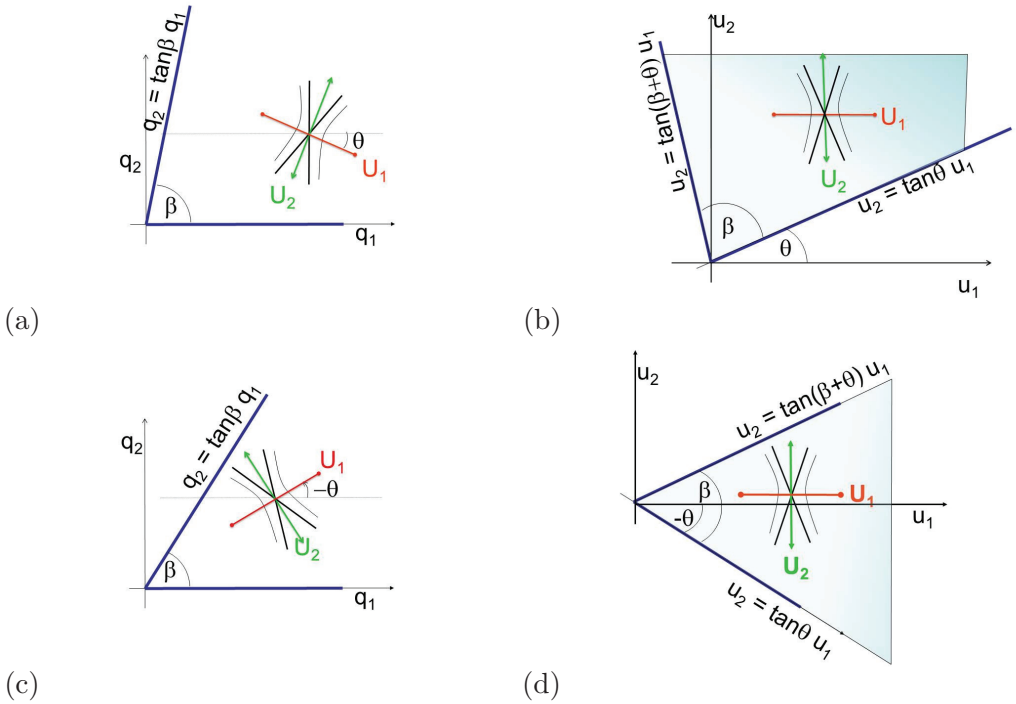

Figure 2. *The saddle in a corner geometry in the configuration space. The potential level sets near the saddle are schematically drawn. The zero level lines are the thick black lines, whereas the thin black curves are the nearly zero potential level lines. The projection of the center eigenspace is denoted by the red line, and that of the stable and unstable eigenspaces is denoted by the green line. The top (bottom) panels show the geometry when θ is positive (negative). The left (right) panels show the geometry in the mass scaled (q_1, q_2) (the rotated (u_1, u_2)) coordinates. The region $\mathcal{A}_L$ is indicated by grey shading.*

the zero level lines of V_a. Since the potential V_a has a saddle point at $q = q_s$, there are two directions, $Q^{\pm} = U_1 + \alpha^{\pm} U_2$, along which V_a vanishes $V_a(q_s + tQ^{\pm}) = 0$ for all t, and $\alpha^{\pm}$ are finite and nonvanishing (see Figure 2).

To simplify further calculations it is convenient to transform the Hamiltonian to its linear normal form. Let us denote by $(\cos\theta, -\sin\theta)^T$ the unitary eigenvector U_1, assuming, with no loss of generality, that $-\pi/2 < \theta \leq \pi/2$. Then $(\sin\theta, \cos\theta)^T$ is the unitary eigenvector U_2. A useful standard observation for natural mechanical Hamiltonians is that rotations of the configuration space can be easily incorporated into the Hamiltonian. Indeed, defining the standard rotation matrix

$$R_\theta = \begin{pmatrix} \cos(\theta) & -\sin(\theta) \\ \sin(\theta) & \cos(\theta) \end{pmatrix} \tag{4.1}$$

and making the symplectic transformation $(q, p) \to (u, v) = (R_\theta q, R_\theta p)$, the Hamiltonian (3.3) becomes

$$H(u, v; b, c, \varepsilon) = \frac{v^2}{2} + \frac{1}{2}(u - R_\theta q_s)^T R_\theta A R_{-\theta}(u - R_\theta q_s) + bV_b(R_{-\theta}u, \varepsilon) + cV_{farfield}(R_{-\theta}u), \tag{4.2}$$

where the quadratic part is diagonal:

$$R_\theta A R_{-\theta} = \begin{pmatrix} \omega^2 & 0 \\ 0 & -\lambda^2 \end{pmatrix}. \tag{4.3}$$

The integrable part of the Hamiltonian (3.3) becomes (where $u_s = R_\theta q_s$)

$$H_{lin} = \frac{v_1^2 + v_2^2}{2} + \frac{\omega^2}{2}(u_1 - u_{1,s})^2 - \frac{\lambda^2}{2}(u_2 - u_{2,s})^2. \tag{4.4}$$

Recall that the quadratic (or, more generally, the integrable) approximation inside the corner is expected to hold only in the reaction zone where the far-field contribution is small. We thus define a bounded corner region in the (u_1, u_2) plane, $\mathcal{A}_L$, and study the dynamics in this region (see Figure 2). The lower and upper boundaries of $\mathcal{A}_L$ are the two rays that emanate from the origin and are aligned with the vectors $(\cos\theta, \sin\theta)$ (lower boundary) and $(\cos(\beta+\theta), \sin(\beta+\theta))$ (upper boundary). This β-wedge is then intersected by the square $[-L, L] \times [-L, L]$, where $L > \max(u_{1,s}, u_{2,s})$. Since $\beta \in (0, \pi/2)$, we have $\beta + \theta \in (-\pi/2, \pi)$ and two cases appear. For $\beta + \theta < \pi/2$ (see Figure 2(d))

$$\mathcal{A}_L = \{u_1 \in [0, L], u_2 \in [u_1 \tan\theta, \min\{u_1 \tan(\beta+\theta), L\}]\}, \tag{4.5}$$

whereas for $\beta + \theta > \pi/2$ (see Figure 2(b))

$$\mathcal{A}_L = \{u_1 \in [0, L], u_2 \in [u_1 \tan\theta, L]\} \cup \{u_1 \in [\operatorname{cotan}(\beta+\theta), L], u_2 \in [0, L]\}. \tag{4.6}$$

Finally, we describe in geometrical terms the well-known structure of the linear flow in $\mathcal{A}_L$. The motion under this linear flow occurs on surfaces defined by the joint levels of H_{lin} and the action I_1:

$$I_1(u_1, v_1) = \frac{v_1^2}{2} + \frac{\omega^2}{2}(u_1 - u_{1,s})^2. \tag{4.7}$$

The action I_1 is the constant of motion associated with the oscillatory motion. The other constant of motion

$$D_2(u_2, v_2) = \frac{v_2^2}{2} - \frac{\lambda^2}{2}(u_2 - u_{2,s})^2 = H_{lin} - I_1 \tag{4.8}$$

determines the hyperbolic motion in the (u_2, v_2) plane. The surface on which the motion occurs, $\{(u, v) | H_{lin}(u, v) = h,\ I_1(u, v) = k\}$, is composed, for $k > 0$ and $h \neq k$, of two disconnected two-dimensional cylinders: the direct product of an ellipse in the (u_1, v_1) plane and two branches of a hyperbola in the (u_2, v_2) plane. The sign of $D_2 = h - k$ determines the nature of the hyperbolic motion. For negative D_2 the hyperbola branches are directed sideways, one having positive $u_2 - u_{2,s}$ and the other having negative $u_2 - u_{2,s}$; see the shaded region in Figure 3. Trajectories belonging to level sets with $D_2 < 0$ do not cross the 3-plane $u_2 = u_{2,s}$: they approach it and then return to the same side. Keeping in mind the chemical origin of our model, we shall say that the motion corresponding to such trajectories occurs "without reaction." On the other hand, if D_2 is positive, branches of the hyperbola extend

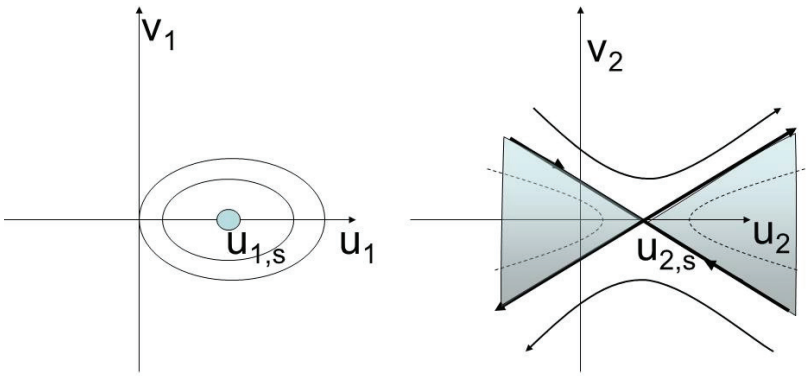

Figure 3. *The phase space structure of the linear system. Shaded region with dashed level curves correspond to nonreacting orbits having $D_2 < 0$ (these trajectories cannot pass the dividing configuration-space section $u_2 = u_{2,s}$).*

horizontally along the full u_2 axis. All the trajectories that belong to level sets with $D_2 > 0$ cross the surface $u_2 = u_{2,s}$. The upper branch of the hyperbola corresponds to orbits with a monotonically increasing u_2 ("reactants to products"), whereas the lower one corresponds to monotonically decreasing u_2 ("products to reactants"). We thus say that such trajectories "realize the reaction."

The level sets on which $H_{lin} = h = k = I_1$ (so $D_2 = 0$) are the singular level sets. These sets separate the two types of motion (with vs. without reaction). Each such singular level set contains a normally hyperbolic Lyapunov periodic orbit $\gamma_h = \{I_1 = h > 0,\ u_2 = u_{2,s},\ v_2 = 0\}$ belonging to the center plane E^c along with its stable and unstable manifolds $W^{s,u}(\gamma_h)$ (each being a straight cylinder). At $h = 0$ this singular level set contains only the saddle-center point P and its stable and unstable manifolds $W^{s,u}(P = \gamma_0)$ (each being a straight line). The projection of these local stable and unstable manifolds ($W^{s,u}(P)$) onto the configuration space is a straight line, aligned with the vector U_2. This projected line is divided by the saddle point u_s into two rays: the extension of the lower ray, the projection of $W^{s,u}_-(P)$, intersects the lower boundary of the corner, whereas the extension of the upper ray, the projection of $W^{s,u}_+(P)$, intersects (if $\tan(\theta + \beta) > 0$) the upper boundary of the corner (see right panels of Figure 2). The projection onto the configuration space of the stable and unstable manifolds of a Lyapunov orbit γ_h with $h > 0$ appears as a collection of many oscillatory orbits that are centered around this line. The projection of the Lyapunov periodic orbit γ_h lies within the corner region, provided h is smaller than $h_{crit-\gamma}$:

$$h_{crit-\gamma} = \min\left\{\frac{\omega^2}{2}(u_{2,s}/\tan(\beta+\theta) - u_{1,s})^2, \frac{\omega^2}{2}(u_{2,s}/\tan\theta - u_{1,s})^2\right\}. \tag{4.9}$$

For large h values, the impacts destroy these periodic orbits. Hereafter we always consider energies that are close to the saddle point energy and are thus strictly smaller than $h_{crit-\gamma}$.

Summarizing, for any given h, the energy surface $H_{lin} = h$ is foliated by the levels of I_1

into the level sets on which the motion occurs. For $h < 0$, all these level sets have negative D_2; hence, they do not cross the surface $u_2 = u_{2,s}$ and no reaction may occur there. When $h > 0$ the energy surface contains, additionally, a Lyapunov saddle periodic orbit with action $I_1(\gamma_h) = h$ and level sets with $0 \le I_1 < I_1(\gamma_h)$. These level sets have positive D_2, and thus orbits belonging to them correspond to reacting trajectories; namely, these orbits belong to the reaction tubes.

See [34] for a detailed explanation of the very similar analogous geometry of the energy surfaces near saddle-center-center-..-center points in the higher-dimensional settings and when higher order terms of the nonresonant normal forms are incorporated. Here we concentrate on the two degrees of freedom case: the higher-dimensional saddle-multicenter case with impacts may be studied similarly, leading to more complicated dynamics (involving, for example, homoclinic orbits to invariant tori as in [35]).

4.2. The impacts. In the rest of this paper we study how the standard integrable behavior changes when the trajectories of the linear system are reflected from the walls of the billiard corner. Here we recall the reflection law from the lower and upper boundaries of the corner region.

The unit vector defining the upper boundary of the corner in the (u_1, u_2) plane is $\mathbf{s}_{\beta+\theta} = (\cos(\beta+\theta), \sin(\beta+\theta))^T$, and its inward normal is $\mathbf{n}_{\beta+\theta} = (\sin(\beta+\theta), -\cos(\beta+\theta))^T$. The resulting reflection law is

$$\begin{aligned} &\mathbf{v} = (v_1, v_2) \\ &\mapsto (v_1 \cos 2(\beta+\theta) + v_2 \sin 2(\beta+\theta), v_1 \sin 2(\beta+\theta) - v_2 \cos 2(\beta+\theta)). \end{aligned} \tag{4.10}$$

It is defined for velocities that exit the corner region, namely those satisfying $\langle \mathbf{v}, \mathbf{n}_{\beta+\theta} \rangle < 0$. Similarly, for the lower ray, $\mathbf{s}_\theta = (\cos\theta, \sin\theta)^T$ and $\mathbf{n}_\theta = (-\sin\theta, \cos\theta)^T$, so the reflection law becomes

$$\begin{aligned} &\mathbf{v} = (v_1, v_2) \\ &\mapsto (v_1 \cos(2\theta) + v_2 \sin(2\theta), v_1 \sin(2\theta) - v_2 \cos(2\theta)). \end{aligned} \tag{4.11}$$

Remark 4.1. *The reflection law preserves energy, namely the integral H. However, reflections from the lower boundary (respectively, upper boundary) do* not *preserve the integrals I_1 and D_2 whenever $\theta \neq 0, \pi/2$ (respectively, whenever $\beta + \theta \neq 0, \pi/2$).*

The change in the integrals by the reflections leads to the nontrivial behavior of the impact system.

4.3. The geometrical parameters. We show in sections 5–6 that the dynamics of the limiting system depend in an essential way on the location and orientation of the saddle point with respect to the corner. The coordinates of the saddle point $u_s = R_\theta q_s$, the angle β of the corner, the ratio ω/λ, and the angle θ between the eigenvector U_1 and the q_1-axis all matter in an essential way in determining the dynamics.

These geometrical parameters, $(\beta, u_s, L, \theta, \omega, \lambda, b, \varepsilon)$, may be extracted numerically from any potential surface describing triatomic reactions. First, one finds the saddle point location q_s and linearizes the vector field at this point to obtain the matrix A. The angle θ may be

calculated via A's entries a_{ij}:

$$\tan\theta = -\frac{2a_{12}}{\sqrt{(a_{11}-a_{22})^2+4a_{12}^2}+a_{11}-a_{22}}.$$

The location of the saddle point in the normal coordinates is then found via $u_s = R_\theta q_s$ (see (4.1)). The estimates of b, ε may be extracted from the diatomic potentials: these parameters are determined by the form of the strong atomic repulsion at short distances. Estimating the linear zone range L may be more delicate. In principle, comparing the approximation (4.4) to the numerical potential energy surface provides the range of validity of the linear approximation. If it appears to be too small, it is possible to extend our theory by including higher order terms of the integrable normal form near the saddle-center (as explained in detail, in another context, for the high-dimensional chemical reaction settings in [34]). The application of this scheme to concrete reactions is currently under study.

A detailed classification of all possible dynamical behaviors for various $(\beta, u_s, L, \theta, \omega, \lambda, b, \varepsilon)$ and h in the symmetric and asymmetric cases is beyond the scope of the current paper (moreover, it is hardly possible at all). In section 5 we analyze the nearly perpendicular behavior (θ nearly zero or, equivalently, $\theta+\beta$ close to zero). In section 6 we provide a rough classification for the dependence of the manifolds' geometry on ω/λ.

5. The nearly perpendicular dynamics. Recall that the projections of $W_-^{s,u}(P)$, the lower branches of the local stable and unstable manifolds of the saddle-center point P, onto the configuration space are directed downward along the vector U_2. We show next that when U_2 is close to being perpendicular to the lower boundary of the corner (so θ is nearly zero), near-integrable behavior occurs. We establish first that when $\theta = \varepsilon = c = 0$ the limit motion in some region containing the saddle-center point is integrable. We then prove that when $\theta \neq 0$ the picture changes dramatically, sometimes leading to chaotic dynamics and sometimes to stable triatomic periodic motion. The same results apply to the upper branches of the manifolds when $(\beta+\theta)$ is small. These two cases may arise, for example, in light-heavy-light reactions (β is close to $\pi/2$) with late (small θ) or early (small $(\beta+\theta)$) barriers.

5.1. Integrable behavior of the perpendicular limit system. When $\theta = \varepsilon = c = 0$ and the energy h is smaller than $h_{crit-\gamma}$ (see (4.9)), homoclinic loops are created by $W_-^{s,u}(\gamma_h)$. Indeed, as shown below, the projection of the stable and unstable manifolds of the center-saddle point P (respectively, of the Lyapunov orbit γ_h) is a straight line (a cylinder) which is perpendicular to the lower boundary of the billiard corner. Thus, after one reflection these manifolds coincide; see Figure 4.

Proposition 5.1. *Consider the limit system ($\varepsilon = c = 0$) at $\theta = 0$ at an energy level $h \in [0, h_{crit-\gamma})$. The lower branch of the unstable manifold of γ_h coincides after reflection with the lower branch of its stable manifold, forming a family of homoclinic orbits to γ_h. The flow of this limit system near the surface of homoclinic orbits is locally integrable: all nearby orbits belonging to the same energy surface h either belong to invariant tori or leave the homoclinic loop region after one round to the $u_2 > u_{2,s}$ region.*

Proof. We first prove the existence of a homoclinic orbit for $h = 0$, where $\gamma_{h=0} = P$. For the case $\theta = 0$ the projection of the stable/unstable manifolds of P onto the configuration

space (u_1, u_2) is a line perpendicular to the line $u_2 = 0$. Indeed, the linear system

$$\dot{u}_1 = v_1, \quad \dot{u}_2 = v_2, \quad \dot{v}_1 = -\omega^2(u_1 - u_{1,s}), \quad \dot{v}_2 = \lambda^2(u_2 - u_{2,s}) \tag{5.1}$$

has the flow

$$\begin{aligned} u_1(t) - u_{1,s} &= (u_1^0 - u_{1,s})\cos(\omega t) + \frac{v_1^0}{\omega}\sin(\omega t), \\ v_1(t) &= -\omega(u_1^0 - u_{1,s})\sin(\omega t) + v_1^0\cos(\omega t), \\ u_2(t) - u_{2,s} &= (u_2^0 - u_{2,s})\cosh(\lambda t) + \frac{v_2^0}{\lambda}\sinh(\lambda t), \\ v_2(t) &= \lambda(u_2^0 - u_{2,s})\sinh(\lambda t) + v_2^0\cosh(\lambda t). \end{aligned} \tag{5.2}$$

So, the stable $W^s(P)$ and unstable $W^u(P)$ one-dimensional manifolds of the equilibrium P are the straight lines $\{u_1 = u_{1,s}, v_1 = 0, u_2 = u_{2,s} - v_2/\lambda\}$ and $\{u_1 = u_{1,s}, v_1 = 0, u_2 = u_{2,s} + v_2/\lambda\}$, respectively. Each straight line is divided by the point P into two rays $W_+^{u,s}(P)$ and $W_-^{u,s}(P)$. The lower rays $W_-^{u,s}(P)$ intersect the wall $u_2 = 0$ (and the other rays intersect either the upper box boundary or the upper corner boundary). The stable and unstable rays that hit the lower wall intersect it at two different phase space points $m_s = (u_{1,s}, 0, 0, \lambda u_{2,s})$ and $m_u = (u_{1,s}, 0, 0, -\lambda u_{2,s})$, respectively (recall that $u_{1,s}, u_{2,s}$ are both positive for sufficiently small θ). We choose, near each of these two points, sufficiently small three-dimensional cross-sections to trajectories in the phase space $N^{s,u} = \{(u, v) | u_2 = 0, ||(u, v) - m_{s,u}|| < \delta\}$. Each of these cross-sections is foliated into 2-disks $N_h^s = N^s \cap \{H = h\}$, $N_h^u = N^u \cap \{H = h\}$. As coordinates on the disk N_h^s we take (u_1, v_1), since the third coordinate v_2 on N^s is expressed from H : $v_2 = \sqrt{2h - (v_1^2 + \omega^2(u_1 - u_{1,s})^2) + \lambda^2(u_{2,s})^2} = \sqrt{2h - 2I_1 + \lambda^2(u_{2,s})^2}$. The same coordinates $(\hat{u}_1, \hat{v}_1)$ work for N_h^u, where the $\hat{v}_2$-coordinate has the same form as v_2 but with a "$-$" sign in front of the root. If a trajectory of the linear flow hits N_h^u, it is transformed to N_h^s due to the reflection law (see (4.11)): the coordinates u_1, u_2, v_1 at the incidence point remain the same, but $v_2 = \dot{u}_2$ changes its sign. This means that the reflection law defines the symplectic global map (gluing map) $S_h : N_h^u \to N_h^s$ as follows: $u_1 = \hat{u}_1$, $v_1 = \hat{v}_1$. In particular, m_u is transformed to m_s: we get a homoclinic orbit Γ to P.

More generally, since $\theta = 0$, for any trajectory hitting[7] the 3-plane $u_2 = 0$, S_h simply changes the sign of v_2. In particular, S_h preserves the energy and the integrals of motion $\hat{I}_1 = I_1(\hat{u}_1, \hat{v}_1) = I_1(u_1, v_1) = k$ and $D_2(u_2, v_2) = h - k = \hat{D}_2$. Thus, trajectories belonging to the level set $\hat{I}_1(\hat{u}, \hat{v}) = k$, $H_{lin}(\hat{u}, \hat{v}) = h$ that hit the lower boundary remain, after reflection, on the same level set with $I_1(u, v) = \hat{I}_1 = k$ and $D_2 = h - k = \hat{D}_2$: the reflection just changes its relative position along the same level set of the integrable linear system (see Figure 4).

Thus, for $h \in (0, h_{crit-\gamma})$, the stable ($I_1 = h$, $D_2 = 0$) and unstable ($\hat{I}_1 = h$, $\hat{D}_2 = 0$) manifolds of the Lyapunov periodic orbit γ_h are cylinders that coincide after one reflection. Moreover, since $\beta < \pi/2$, these cylinders hit the 3-plane $u_2 = 0$ at u_1 values that are bounded away from 0, namely bounded away from the corner.

The dynamics for trajectories near the homoclinic loops are also fairly simple. In particular, trajectories lying on the given level set $H = h$, $I_1 = k$ are projected onto the plane

[7] In other words, trajectories arriving to this section with $\hat{v}_2 < 0$.

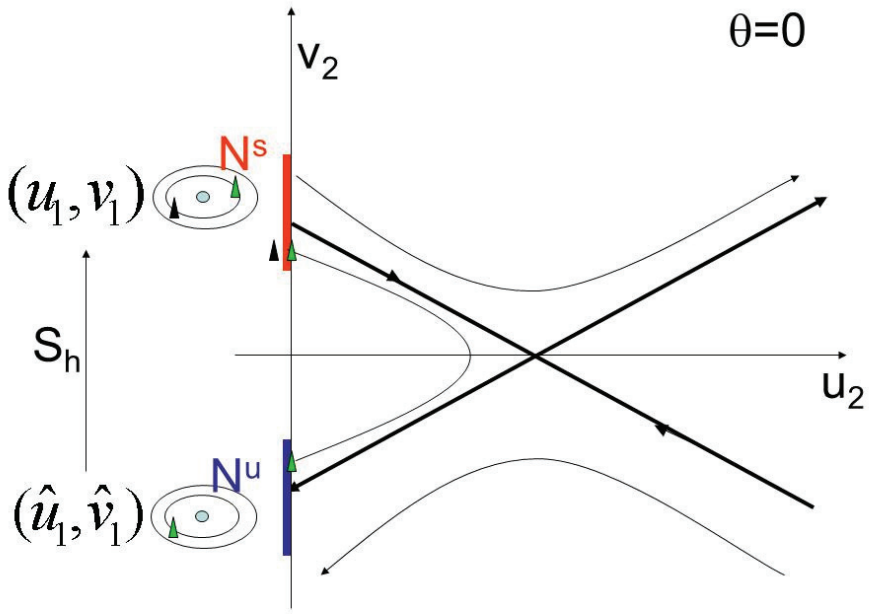

Figure 4. *The return map for $\theta = 0$. The green triangle on N^s is mapped by the smooth flow to the green triangle on N^u. Its reflection (the S_h image) is the black triangle belonging to N^s. Here, it belongs to the same level sets I_1, D_2, yet its velocity v_2 changes sign.*

(u_2, v_2) into one of the two hyperbola branches of $D_2 = h - k$. If $h - k < 0$ and $u_2 < u_{2,s}$, then trajectories starting on N^s move towards P and then return to the cross-section N^u. In other words, the reflection law glues this hyperbola-like branch into a closed curve (see Figure 4: the green triangle on N^s is mapped by the flow to the green triangle on N^u and then reflects to the black triangle, namely, back to N^s). Since such orbits also belong, in the (u_1, v_1) plane, to the closed curve $I_1 = k$, these orbits belong, topologically, to an invariant torus in the phase space. Similarly, trajectories for which $D_2 = h - k > 0$ belong to two disjoint cylinders (direct product of the circle $I_1 = k$ in the (u_1, v_1) plane and the two branches of the corresponding hyperbola in the (u_2, v_2) plane). Here, the gluing map defined by the reflection law glues the two end circles (those intersecting the section $u_2 = 0$) of these cylinders. Trajectories move along one of the cylinders towards the section $u_2 = 0$ and after the first reflection escape along the second cylinder to the region $u_2 > u_{2,s}$. Their global dynamics, after they pass the saddle point, depend on $(\beta, u_s, \omega, \lambda)$ as discussed in section 6. ■

We conclude that for $\theta = \varepsilon = c = 0$ the motion near Γ in the region $u_2 < u_{2,s}$ is indeed simple. For negative energy h, the motion near[8] the homoclinic loop occurs within the solid torus $0 \le I_1 \le I_1^*$, $D_2 = h - I_1 \le 0$. The motion is quasi-periodic if the rotation number on the related invariant 2-torus is irrational, and it is periodic if this number is rational.[9] Inside

[8] Namely, for small enough $I_1^*, -h$.

[9] The same behavior extends to all energies in $-\frac{\lambda^2}{2}(u_{2,s})^2 < h \le 0$, but here we are concerned with the near saddle-center behavior.

this solid torus there is also a unique elliptic periodic orbit $I_1 = 0$, $D_2 = h$. For $h = 0$, this periodic orbit is replaced by the homoclinic orbit Γ. When $h > 0$, the orbits with negative D_2 are again periodic or quasi-periodic. On the other hand, the orbits with positive D_2 cross into the $u_2 > u_{2,s}$ region. Their behavior may be rather complicated since they may hit the upper boundary of the billiard which is slanted. For sufficiently small h, such trajectories closely follow $W_+^{u,s}(P)$, the upper branches of the stable and unstable manifolds of P. Hence, the global structure of $W_+^{u,s}(P)$ determines their behavior.

We say that $W_+^{u,s}(P)$ exhibit simple dynamics if these manifolds intersect the upper boundary at a monotonically increasing sequence of u until exiting the corner region; see Figure 6 and the first column of Figure 7. Otherwise, we say that their behavior is complicated; see the second and third columns of Figure 7. We see that in the complicated cases the manifolds return to the corner region, possibly hitting both boundaries and possibly hitting the boundaries at some $u_1 < u_{1s}$. We describe next the behavior of $W_-^{u,s}(P)$ and of trajectories in their neighborhood near a slightly slanted lower boundary, and we discuss the behavior of the trajectories at $u_2 > u_{2,s}$ in section 6.

We should note that the behavior of trajectories with a larger oscillatory component (e.g., trajectories starting near $u_{2,s}$ with $I_1 > h_{crit-\gamma}$) is expected to be complicated as well: almost always such trajectories eventually hit the upper ray, and we expect that this reflection would, almost always, destroy the integrability. Notice that such reflections, induced by the geometry, supply an alternative route for the creation of reactions which is unrelated to the local structure near P. We will return to this point in the discussion.

5.2. Nonintegrable behavior. We establish next that for small enough nonzero θ the motion in the limit system is chaotic for a range of energies. We then prove that similar behavior occurs for sufficiently small ε, c. More precisely, we prove below the existence of transverse homoclinic orbits to a saddle periodic orbit (Poincaré homoclinic orbits). To this aim we use some of the ideas developed in [30, 31], where the center-saddle case was analyzed (the first discussion of the problem was in [29]). The chaotic nature of the motion follows from this result: it is well known that near such homoclinic orbits there is an invariant subset which is described on some cross-section by a transitive Markov chain, so in particular, this set contains a countable set of saddle periodic orbits, almost periodic orbits, etc. [36, 37].

Theorem 5.2 (complicated dynamics I). *If $|\theta|$ is nonzero and sufficiently small, then, for $\varepsilon = c = 0$, the system (3.3) admits the following properties:*

1. *The lower branches of the stable and unstable separatrices of P are split.*
2. *There is a critical energy value h^0, depending on the geometrical parameters $(\theta, u_s, \lambda, \omega)$, satisfying $0 < h^0 < h_{crit-\gamma}$, such that at energies $h \in (h^0, h_{crit-\gamma})$ the Lyapunov periodic orbit γ_h has two* transverse *homoclinic orbits.*
3. *At the energy level $H = h^0(\theta, u_s, \lambda, \omega)$ the flow has a tangent homoclinic orbit to the related Lyapunov periodic orbit.*
4. *For $0 < h < h^0$ the lower branches of the separatrices do not admit simple[10] homoclinic orbits to γ_h.*

Proof. 1. We construct, as in the proof of Proposition 5.1, the global map that is defined by the reflection law from the slightly slanted bottom wall. Let $\mu = \tan\theta$ and

[10] Orbits that reflect only once from the corner boundaries.

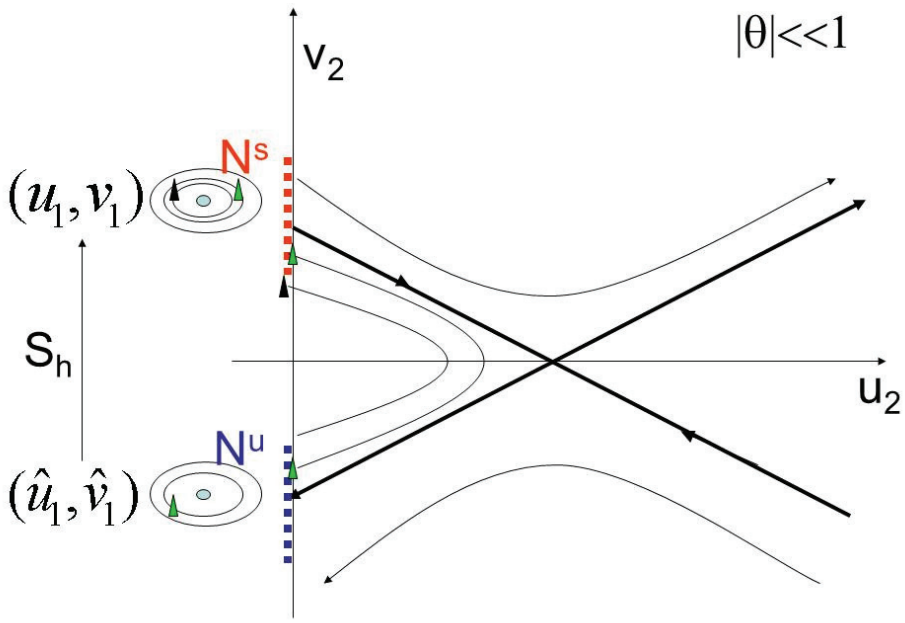

Figure 5. *The return map for small θ. As in Figure 4, the image of the green triangle of N^s under the flow and the gluing map is the black triangle. Here, the velocities (v_1, v_2) and the corresponding level sets I_1, D_2 are changed due to the reflection.*

$\mathbf{s} = (1/\sqrt{1+\mu^2} = \cos\theta, \mu/\sqrt{1+\mu^2} = \sin\theta)^T$ be, as above, a unit vector defining the lower boundary of the corner. Then, for sufficiently small θ, the 3-plane given by $u_2 = \mu u_1$ provides a cross-section to the linear flow. Recall that the projections of the lower branches of the local stable and unstable manifolds of P, $W^{u,s}_-(P)$, are straight lines. Their extensions intersect the bottom wall[11] at the points $m_s = (u_{1,s}, \mu u_{1,s}, 0, \lambda(u_{2,s} - \mu u_{1,s}))$ and $m_u = (u_{1,s}, \mu u_{1,s}, 0, -\lambda(u_{2,s} - \mu u_{1,s}))$. As before, we consider some small cross-sections N^s, N^u near these points; see Figure 5. They are again foliated into 2-disks N^s_h, N^u_h. The coordinates on these cross-sections are (u_1, v_1), where here $u_2 = \mu u_1$, and v_2 is expressed from $H : v_2 = \pm\sqrt{2h - 2I_1 + \lambda^2(\mu u_1 - u_{2,s})^2}$. The sign "+" corresponds to N^s_h and the sign "−" to N^u_h. The restriction of the 2-form $dv_1 \wedge du_1 + dv_2 \wedge du_2$ to N^s_h (and similarly for N^u_h) is now given as $dv_1 \wedge du_1 + \mu dv_2 \wedge du_1$, where v_2 is taken from H. Applying the reflection law from the slanted wall boundary (4.11) to values $(\hat{u}_1, \hat{v}_1) \in N^u_h$, we obtain the gluing symplectic map $S_h : N^u_h \to N^s_h$ (with respect to the nontrivial symplectic form; see the appendix):

$$S_h : (\hat{u}_1, \hat{v}_1) \mapsto \left(\hat{u}_1, \frac{(1-\mu^2)\hat{v}_1 + 2\mu\hat{v}_2}{1+\mu^2}\right) = (\hat{u}_1, \hat{v}_1 \cos 2\theta + \hat{v}_2 \sin 2\theta). \tag{5.3}$$

This gluing map is defined for trajectories pointing down so that $-\mu\hat{v}_1 + \hat{v}_2 < 0$. Namely, for sufficiently small $|\mu|$ we require that $\hat{v}_2 < 0$, so the sign in front of the radical for $\hat{v}_2$ should be negative.

[11] Recall that since θ is small, $u_{1,s}$ and $u_{2,s}$ are positive.

We now prove the first assertion of the theorem. We show that the reflection of the unstable branch ($W^u_-(P)$) from the lower boundary (the S_0-image of the point m_u) does not coincide with the stable branch ($W^s_-(P)$) intersection with this boundary (the point m_s). For S_0 we should set $\hat{u}_1 = u_{1,s}$, $\hat{v}_1 = 0$, $\hat{v}_2 = -\lambda(u_{2,s} - \mu u_{1,s})$. Then we get for $\mu \neq 0$

$$u_1 = u_{1,s}, \quad v_1 = \frac{-2\mu\lambda(u_{2,s} - \mu u_{1,s})}{1+\mu^2} = -2\mu\lambda u_{2,s}(1 + O(\mu)) \neq 0,$$

and therefore the stable and unstable manifolds of P are split: They are of order μ apart.

2–3. Now, let us fix $h > 0$. We first show that the intersection of $W^s_-(\gamma_h)$ (the lower branch of the stable manifold of the Lyapunov periodic orbit γ_h) with N^s_h is an ellipse. We then show that the S_h-image of the intersection of the unstable manifold branch $W^u_-(\gamma_h)$ with N^u_h is another ellipse. We then prove that these two ellipses intersect as the energy is increased beyond a critical energy. Recall that for $0 < h < h_{crit-\gamma}$ the intersections of $W^{s,u}_-(\gamma_h)$ with $N^{s,u}$ are bounded away from the corner[12] and occur, for sufficiently small $|\mu|$, with a vertical velocity which is strictly bounded away from 0. We consider here only such h values.

First, note that the two-dimensional cylinders $W^{s,u}_-(\gamma_h)$ are given by solutions of the two equations $I_1(u_1, v_1) = v_1^2/2 + \omega^2(u_1 - u_{1,s})^2/2 = h$, $v_2 = \pm\lambda(u_{2,s} - u_2)$, where the $+/-$ signs correspond to the stable/unstable manifolds. The intersection of $W^s_-(\gamma_h)$ with N^s (with coordinates (u_1, v_1, v_2)) is the closed curve $I_1(u_1, v_1) = h$, $v_2 = \lambda(u_{2,s} - \mu u_1)$, and its projection onto the (u_1, v_1) plane is an ellipse. Similarly, $W^u(\gamma_h)$ intersects N^u (with coordinates $(\hat{u}_1, \hat{v}_1, \hat{v}_2)$) along the closed curve $I_1(\hat{u}_1, \hat{v}_1) = h$, $\hat{v}_2 = -\lambda(u_{2,s} - \mu\hat{u}_1)$, and its projection onto the $(\hat{u}_1, \hat{v}_1)$ plane is an ellipse as well.

To find the intersection of the S_h-image of the trace of $W^u_-(\gamma_h)$ with the trace of $W^s_-(\gamma_h)$, it is convenient to use the action-angle (here simply polar) coordinates (I_1, φ) on N^s_h and $(\hat{I}_1, \psi)$ on N^u_h : $v_1 = \sqrt{2I_1}\cos\varphi$, $u_1 = u_{1,s} + \sqrt{2I_1/\omega^2}\sin\varphi$, $\hat{v}_1 = \sqrt{2\hat{I}_1}\cos\psi$, $\hat{u}_1 = u_{1,s} + \sqrt{2\hat{I}_1/\omega^2}\sin\psi$. Using (5.3), the equation $S_h(\hat{u}_1, \hat{v}_1) = (u_1, v_1)$ becomes

$$\begin{aligned} &u_{1,s} + \sqrt{2h/\omega^2}\sin\varphi = u_{1,s} + \sqrt{2h/\omega^2}\sin\psi, \\ &\sqrt{2h}\cos\varphi = \frac{(1-\mu^2)\sqrt{2h}\cos\psi - 2\mu\lambda[u_{2,s} - \mu(u_{1,s} + \sqrt{2h/\omega^2}\sin\psi)]}{1+\mu^2}. \end{aligned}$$

The first equation implies that either $\varphi = \psi$ or $\varphi = \pi - \psi$. In the first case we obtain the following equation for φ:

$$\mu\sqrt{2h}\left(\cos\varphi - \frac{\lambda}{\omega}\sin\varphi\right) = -\lambda(u_{2,s} - \mu u_{1,s}),$$

which has no solutions for sufficiently small $|\mu|$. In the second case the equation for φ becomes

$$\sqrt{2h}\left(\cos\varphi - \mu^2\frac{\lambda}{\omega}\sin\varphi\right) = -\mu\lambda(u_{2,s} - \mu u_{1,s}). \tag{5.4}$$

[12]More precisely, these are bounded away from the 2-plane $(u_1 = 0, u_2 = \mu u_1 = 0, v_1, v_2)$ which corresponds to the corner in the phase space.

Defining

$$\sigma = \frac{\omega^2\lambda^2(u_{2,s} - \mu u_{1,s})^2}{2(\omega^2 + \mu^4\lambda^2)} = \frac{(\lambda u_{2,s})^2}{2} + O(\mu),$$

we see that for a fixed μ (5.4) has no solutions for $0 < h < \sigma\mu^2$, has a unique solution at $\sigma\mu^2$, and has two solutions for $h \in (\sigma\mu^2, h_{crit-\gamma})$. Indeed, notice that the S_h-image of the trace of $W^u_-(\gamma_h)$ is given in the (u_1, v_1) coordinates by

$$\begin{aligned} u_1 &= \hat{u}_1, \\ v_1 &= \hat{v_1}\cos 2\theta + \hat{v}_2 \sin 2\theta = -\lambda u_{2,s}\sin 2\theta + \hat{v_1}\cos 2\theta + \mu\lambda\hat{u}_1 \sin 2\theta; \end{aligned} \tag{5.5}$$

that is, it is a linear transformation of the ellipse, so it is also an ellipse. It follows from the geometry of intersecting ellipses that for $h > \sigma\mu^2$ these two solutions correspond to two transversal homoclinic orbits to the Lyapunov periodic orbit γ_h, and that at the intermediate case

$$h^0 = h^0(\theta, u_s, \lambda, \omega) = \sigma\mu^2 = \frac{(\lambda u_{2,s}\tan\theta)^2}{2} + O((\tan\theta)^3) \tag{5.6}$$

the unique solution corresponds to a tangent homoclinic orbit of γ_h (it corresponds to the outer tangency of the ellipses).

4. Since for $h < h^0$ the two ellipses do not intersect, and since in the corner interior the flow is integrable, the lower branches do not admit simple homoclinic orbits at such energies. In general, it is still possible that consequent reflections of the extensions of $W^{s,u}_-(\gamma_h)$ from the corner boundaries will produce homoclinic orbits. ■

Next, we assert that similar behavior appears when c and ε are sufficiently small and the billiard-like potential indeed limits to the impact flow. More precisely, in [28] we prove that away from a small boundary layer near the billiard boundary, regular reflections of impact flows are C^r close to the corresponding reflection-like segments of the smooth Hamiltonians. The smooth Hamiltonians are assumed to be in the standard mechanical form with potentials that are a sum of a smooth potential and a family of billiard-like potentials (satisfying assumptions I–IV of [27]). Additionally, to obtain the correct impact limit, it is assumed that the value of the full potential along the billiard boundary is strictly positive. Then, for positive ε the Hill region of the smooth flow lies within the billiard region and, near regular impacts, limits to it as $\varepsilon \to 0^+$. Under these conditions it is proved in [28] that for sufficiently small ε the smooth reflection from the Hill region boundary limits to the billiard reflection law. Here, to comply with this latter condition, we assume hereafter that the potential along the corner rays in $\mathcal{A}_L$

$$R_{\beta,L} = \{(u_1, u_2)|\,(u_2 = u_1\tan\theta) \cup (u_2 = u_1\tan(\beta + \theta)) \cap (|u_{1,2}| \le L)\} \tag{5.7}$$

is strictly positive. Namely, we assume that there exist positive constants ε_0, B_1 such that for all $0 < \varepsilon < \varepsilon_0$

$$\left(bV_b(R_{-\theta}u, \varepsilon) + \frac{\omega^2}{2}(u_1 - u_{1,s})^2 - \frac{\lambda^2}{2}(u_2 - u_{2,s})^2\right)_{(u_1,u_2)\in R_{\beta,L}} > B_1. \tag{5.8}$$

For the power law repulsion law (3.5), the first term is infinite, so the inequality is satisfied for any $b > 0$. When the diatomic repulsion is modeled by a bounded potential (e.g., (3.4)),

b should be taken to be sufficiently large so that (5.8) holds. Such an assumption is natural in the chemical-reaction context: the nuclear potential energy associated with small diatomic distances is much larger than the barrier energy. Thus, such an assumption is satisfied by adequate models of the PES of triatomic reactions. Then, by [28], we can establish the following.

Theorem 5.3 (complicated dynamics I: smooth case). *Assume that $V_b(q;\varepsilon)$ is a billiard-like potential family limiting to the billiard in the β-wedge, $V_{farfield}(q)$ is bounded in the C^r topology in the corner region, and (5.8) is satisfied. Then, for sufficiently small ε, c, and θ_{max}, for all $0 < |\theta| < \theta_{max}$, the system (3.3) admits the same properties as listed in Theorem 5.2. There, the critical energy levels $h^0, h_{crit-\gamma}$ need to be replaced by a family of (ε, c) dependent critical energies $h^{\varepsilon,c}$ and by $h^{\theta_{max}}_{crit-\gamma}$. Moreover, the critical values at which the tangent homoclinic bifurcation occurs depend smoothly on (ε, c) and approach the limiting bifurcation energy as (ε, c) are decreased to zero: $h^{\varepsilon,c} \to h^0$.*

Proof. Notice that in the proof of Theorem 5.2 for the limit system we may replace the cross-sections N^s with any other locally transverse cross-section to $W^u_-(P)$ in the interior of the domain. Consider, for example, such a local cross-section at $\Sigma^{\bar{u}_2} = \{(u, v) : u_2 = \bar{u}_2 < (u_{2,s} + u_{1,s} \tan\theta)/2\}$. The first intersection of the extensions of $W^{u,s}_-(\gamma_h)$ with $\Sigma^{\bar{u}_2}$ are always transverse for the limit system. $\Sigma^{\bar{u}_2}$ also provides, under specified conditions, a locally transverse cross-section to the image of the first reflection of the extension of $W^u_-(\gamma_h)$ from the lower boundary. Indeed, for any fixed $\bar{u}_2$ one can choose sufficiently small $|\theta|$ and fix an energy level $h^{\bar{u}_2}(\theta)$ so that for all $h \in [0, h^{\bar{u}_2}(\theta)]$ this section is transverse to these orbits. Moreover, $h^{\bar{u}_2}(\theta) \to h_{crit-\gamma}$ monotonically as $|\theta| \to 0$. Thus, the proof of Theorem 5.2 applies, in the limit system, to the traces of $W^{u,s}_-(\gamma_h)$ on $\Sigma^{\bar{u}_2}$ for all $h \in [0, h^{\bar{u}_2}(\theta)]$. Namely, for small $|\theta|$, the trace which corresponds to the first intersection of the extension of $W^s_-(\gamma_h)$ with $\Sigma^{\bar{u}_2}$ and the image of the corresponding trace of $W^u_-(\gamma_h)$ after its first reflection from the lower boundary intersect transversely at $h > h^0$, do not intersect at $h < h^0$, and are tangent at $h = h^0$. Notice that for sufficiently small $|\theta|$, $h^{\bar{u}_2}(\theta)$ is of order one, whereas the θ-dependent homoclinic bifurcation value h^0 is small (see (5.6)); namely, $h^0 \in (0, h^{\bar{u}_2}(\theta))$. Also, recall that in the proof of Theorem 5.2 $|\theta|$ is assumed to be sufficiently small so that the reflection of $W^u_-(\gamma_h)$ from the lower boundary is a regular reflection: it occurs with strictly negative v_2. Let θ_{max} be sufficiently small so that (a) Theorem 5.2 applies, (b) at θ_{max} the homoclinic bifurcation occurs at an energy at which $\Sigma^{\bar{u}_2}$ is transverse as explained above, and (c) this energy is smaller than the nuclear diatomic repulsion energy. Namely, at $\pm\theta_{max}$, $h^0 < h^{\theta_{max}}_{crit-\gamma} := \min(h^{\bar{u}_2}(\pm\theta_{max}), B_1)$. This last condition implies that for sufficiently small (c, ε), the Hill region of (3.3) near the impact point $(u_{1,s}, u_{1,s} \tan\theta)$ limits to the lower ray boundary of the corner for all $h \in [0, h^{\theta_{max}}_{crit-\gamma}]$. Thus, by [28], for all $|\theta| < \theta_{max}$ and $h \in [0, h^{\theta_{max}}_{crit-\gamma}]$, for sufficiently small (c, ε), the stable trace and the image of the unstable trace under the smooth flow are C^r close to the corresponding traces of the impact flow. Hence, the result is established. ∎

Figure 6 demonstrates that for small $|\theta|$ and small ε (at $c = 0$) the lower branch of the unstable manifold of P indeed exhibits complicated behavior.

5.3. Elliptic islands. Theorem 5.2 implies that for any small fixed $\mu = \tan\theta$, the stable and the unstable manifolds of the Lyapunov periodic orbit γ_h with $h^0 = \sigma\mu^2 \approx (\lambda u_{2,s} \tan\theta)^2/2$

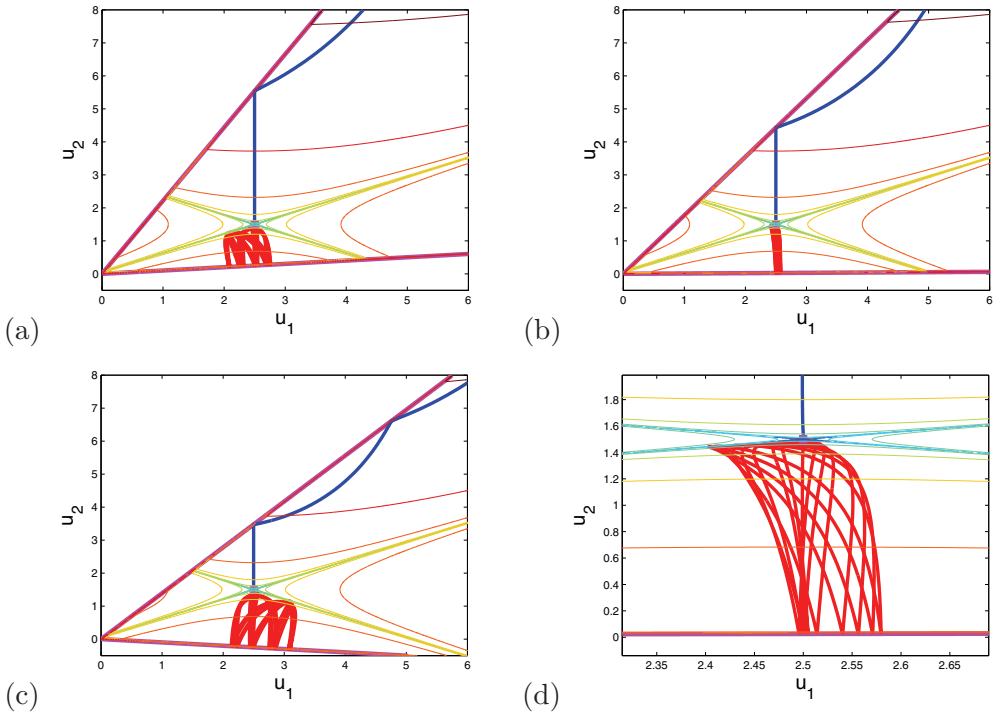

Figure 6. *Projections of the unstable manifold of P onto the configuration space at small θ values.* (a) $\theta = 0.1$. (b) $\theta = 0.01$. (c) $\theta = -0.1$. (d) *Zoom-in of* (b). *Thick blue (red) line: $W^u_+(P)$ ($W^u_-(P)$). Thin colored lines are the level sets of the geometric potential, with the exponential repulsion form (see (3.4)). Here,* $b = 10$, $\varepsilon = 0.01$, $u_s = (2.5, 1.5)$, $\beta = \pi/3$, $\omega^2 = 1$, $\lambda^2 = 3$.

undergo a nondegenerate tangent homoclinic bifurcation. Such a bifurcation leads, in particular, to the creation of elliptic periodic orbits near the tangent homoclinic orbit.

Theorem 5.4 (complicated dynamics II). *At the semi-interval $h > h^0$, for sufficiently small θ, the limit system $(3.3)_{\varepsilon=c=0}$ has a countable set of h-intervals Δ_n accumulating at $h = h^{0+}$ such that for $h \in \Delta_n$ the limit flow has generic elliptic periodic orbits with their period tending to infinity as $n \to \infty$.*

Proof. We show that at $\varepsilon = 0$ one may construct a smooth symplectic return map to a section close to the Lyapunov periodic orbit γ_{h^0}. Then, the classical results regarding the emergence of elliptic islands near homoclinic tangencies are applicable.

In order to formulate the classical results precisely, let us recall some details [38, 39, 40, 41, 42]. Suppose a family of smooth symplectic diffeomorphisms $f_{\bar{c}}$ acts on a symplectic two-dimensional manifold (M, ω). Let p be a saddle fixed point for any parameter value $\bar{c}$ near $\bar{c} = 0$ with eigenvalues $0 < \Lambda(\bar{c}) < 1, \Lambda^{-1}(\bar{c})$. Assume that $f_{\bar{c}}$ undergoes a generic homoclinic bifurcation; at $\bar{c} = 0$ the stable and unstable manifolds of p have a quadratic intersection at some point q (different from p), creating a tangent homoclinic orbit Γ. Furthermore, the unfolding $f_{\bar{c}}$ is generic; namely, in a small neighborhood of Γ there are no simple homoclinic orbits to p at $\bar{c} < 0$ and there are two transversal homoclinic orbits at $\bar{c} > 0$ (or vice versa). Near p one can choose symplectic Darboux coordinates (x, y) in which the 2-form ω casts as

$\omega = dx \wedge dy$. The local representation of the maps for any sufficiently small $\bar{c}$ is

$$x_1 = [\Lambda + f_1(x,y)]x, \quad y_1 = [\Lambda^{-1} + g_1(x,y)]y,$$

with f_1, g_1 being of the first order at $(0,0)$. Recall that points of Γ tend to p as $n \to \pm\infty$ (n is the iteration number of f). Choose two points q_+, q_- of Γ such that $q_+ = (x_+, 0)$ belongs to the segment $x > 0$, $y = 0$ (a piece of W^s) and $q_- = (0, y_-)$ belongs to the segment of W^u, which we assume to be $y > 0$. Then one may take two small neighborhoods V_s of q_+ and V_u of q_- that both belong to the coordinate chart. Then it is clear that points from the semi-neighborhood $y > 0$ of V_s can reach under iterations of f a semi-neighborhood $x > 0$ of V_u for all iterations $n \geq n_0 \geq 1$ (n_0 depends on f, on the locations of q_+, q_-, and on the size of V_s, V_u). The quadratic tangency of W^s and W^u along Γ means in these coordinates that there is some positive integer N such that the global map $f^N : V_u \to V_s$ can be written in V_u in the form $\bar{x} - x_+ = \bar{a}x + \bar{b}(y - y_-) + \cdots$, $\bar{y} = -\bar{b}^{-1}x + \frac{1}{2}Ax^2 + Bx(y - y_-) + \frac{1}{2}C(y - y_-)^2 + \cdots$ with nonzero C. It is known that if $\bar{b} > 0$, $C < 0$, then, at $\bar{c} = 0$, there are no orbits that stay forever in $V_s \cup V_u$ under the action of the first return maps $f^n \circ f^N$ (except of Γ). Suppose, to be definite, that two homoclinic orbits to p appear for small $\bar{c} > 0$.

Theorem 5.5 (see [38, 39, 40, 41, 42]). *In the semi-interval $\bar{c} > 0$ there is a countable set of $\bar{c}$-intervals Δ_n accumulating at $\bar{c} = 0^+$ such that for $\bar{c} \in \Delta_n$ the map $f_{\bar{c}}$ has generic elliptic periodic orbits and their periods tend to infinity as $n \to \infty$.*

Recall that the genericity of an elliptic fixed point or a periodic orbit means that some of its Birkhoff coefficients in the related normal form do not vanish.

For our case, the local map $f_{\bar{c}}$ is obtained as follows. Let (I_1, φ) denote the symplectic polar coordinates on the (u_1, v_1) plane (see above). The semi-interval $\varphi = 0$, $0 < I_1 \leq I_1^0$ is a transverse cross-section. We fix $h = h^0 = \sigma\mu^2$ and choose, for sufficiently small δ, ζ, the 3-disk $Q : \varphi = 0$, $|I_1 - I(\theta)| < \delta$, $|u_2 - u_{2,s}| < \zeta$, $|v_2| < \zeta$, where $I(\theta) = h^0$ is the I_1 action of the periodic orbit γ_{h^0}. This Q is a cross-section to orbits that are close to the periodic orbit γ_{h^0}. The generic family of symplectic maps in the 2-disks Q_h is defined by fixing the levels $H = h$ in Q and by defining the bifurcation parameter $c = h - h^0$. The coordinates on Q_h are (u_2, v_2), and the map in these coordinates is linear in $u_2^0 - u_{2,s}, v_2^0$: it is obtained from (5.2) if we set $t = \frac{2\pi}{\omega}$ in $u_2(t), v_2(t)$. The quarter $D_2 \leq 0$, $u_2 \leq u_{2,s}$ (recall that $u_{2,s} > 0$ for the case under consideration) corresponds to those orbits of the flow which go from N_h^s to N_h^u for positive t. The tangent homoclinic orbit Γ cuts Q_{h^0} transversely, when t increases, along an infinite sequence of points that lie on the semi-interval $D_2 = 0$, $u_2 < u_{2,s}$, $v_2 > 0$ and accumulate to $(u_{2,s}, 0)$—the trace of γ_{h^0} in Q_{h^0}. We fix some point q_+ of this sequence. This orbit also cuts transversely the cross-section $N_{h^0}^s$ at some point q_+^s on the trace of $W^s(\gamma_{h^0})$. Since the time of passage between these two points of transverse intersections is finite, the flow defines a local symplectic map $T_+ : N_{h^0}^s \to Q_{h^0}$ in some small neighborhoods of q_+^s and q_+, respectively.

Similarly, the map T_- is constructed. T_- acts from some neighborhood of q_- on the unstable semi-interval $D_2 = 0$, $u_2 < u_{2,s}$, $v_2 < 0$ to a neighborhood of the trace of Γ on $N_{h^0}^u$. Thus, we have an analytic symplectic map (global map) $T_h = T_+ \circ S_h \circ T_-$ acting from a small neighborhood of q_- to a small neighborhood of q_+. The global map T_{h^0} transforms a small segment of the unstable manifold of the saddle fixed point $(u_{2,s}, 0)$ near $q_- \in Q_{h^0}$ to its image in the neighborhood of q_+. Since Γ is a nondegenerate tangent homoclinic orbit, this image

is quadratically tangent to the stable manifold of the saddle fixed point. Moreover, as the mutual position of the two ellipses shows, this segment belongs to the quarter $D_2 > 0$, $v_2 > 0$, and $u_2 < u_{2,s}$ for it. It means that we realize the case $\bar{b} > 0$, $C < 0$ of the above mentioned theorem, and we get an infinite sequence of intervals in $h > h^0$ corresponding to the existence of elliptic periodic orbits of the system. ■

Theorem 5.6 (complicated dynamics II: smooth). *Under the same conditions of Theorem 5.3, for sufficiently small $|\theta| < \theta_{max}$, ε, and c, at the semi-interval $h > h^{\varepsilon,c}(\theta)$, the system (3.3) has a countable set of h-intervals Δ_n accumulating at $h = h^{\varepsilon,c}(\theta)^+$ such that for $h \in \Delta_n$ the limit flow has generic elliptic periodic orbits with their period tending to infinity as $n \to \infty$.*

Proof. For sufficiently small $|\theta|$, near h^0, the gluing map S_h corresponds to a regular reflection. Thus, under the same conditions as in Theorem 5.3, by [28], for sufficiently small (ε, c), the smooth version of the return map to Q_h, $T_h^{\varepsilon,c}$ is C^r close to T_h for all $|\theta| < \theta_{max}$ and $h \in [0, h^{\theta_{max}}_{crit-\gamma}]$. Hence, by Theorem 5.3, for $h > h^{\varepsilon,c}(\theta)$, where $h^{\varepsilon,c}(\theta)$ denotes the energy of the homoclinic tangent bifurcation of the smooth system, Theorem 5.5 may be applied to the return map $T_h^{\varepsilon,c}$. Moreover, this return map depends smoothly on (ε, c); hence the theorem follows. Notice that the classical results are clearly applicable for finite ε values for which the homoclinic tangency persists. Here, we see that one may change the order of the limits; namely, even for arbitrarily small ε the stability islands appear. ■

6. Criteria for simple dynamics. The behavior near the lower branches of the stable and unstable manifolds of P was shown to be integrable when $\theta = \varepsilon = c = 0$ and nonintegrable for small nonzero θ. Indeed, we proved that the stable and unstable manifolds of γ_h intersect for a range of energy values, $h \in (h^0 \approx \frac{(\lambda u_{2,s} \tan\theta)^2}{2}, h_{crit-\gamma})$. Similar results apply for the upper branches when $(\beta + \theta)$ is small.

Proving analogous results regarding integrability or nonintegrability of the dynamics near P for general $(\beta, u_s, L, \theta, \omega, \lambda)$ is a difficult problem. Rather than seeking the general solution, we identify cases in which the nature of the dynamics can be roughly predicted. More precisely, we classify the behavior of the upper/lower branches of the manifolds as follows.

SD (simple dynamics). For small h, the upper (respectively, lower) branches of the unstable and stable manifolds are reflected to the regions of "no-return" monotonically (with a monotone sequence of reflecting points exiting the corner region), and thus near these branches there are no recurrent trajectories in the neighborhood of P; see the first columns of Figures 7 and 9.

PCBD (possibly complicated bounded dynamics). For small h values, the upper (respectively, lower) branches of the manifolds are trapped in the upper (respectively, lower) corner region: these manifolds cannot exit the corner region from the product (respectively, reactant) channel; see the third columns of Figures 7 and 9.

CD (chaotic dynamics). The branches of the manifolds intersect each other for a range of energy levels that are close to the barrier energy.

The first and second rough criteria check whether the manifolds reflect in a simple, monotone way out of the corner region or whether they are trapped. Clearly SD imply that no chaotic behavior is possible for the corresponding branches. Folding back of the manifolds is

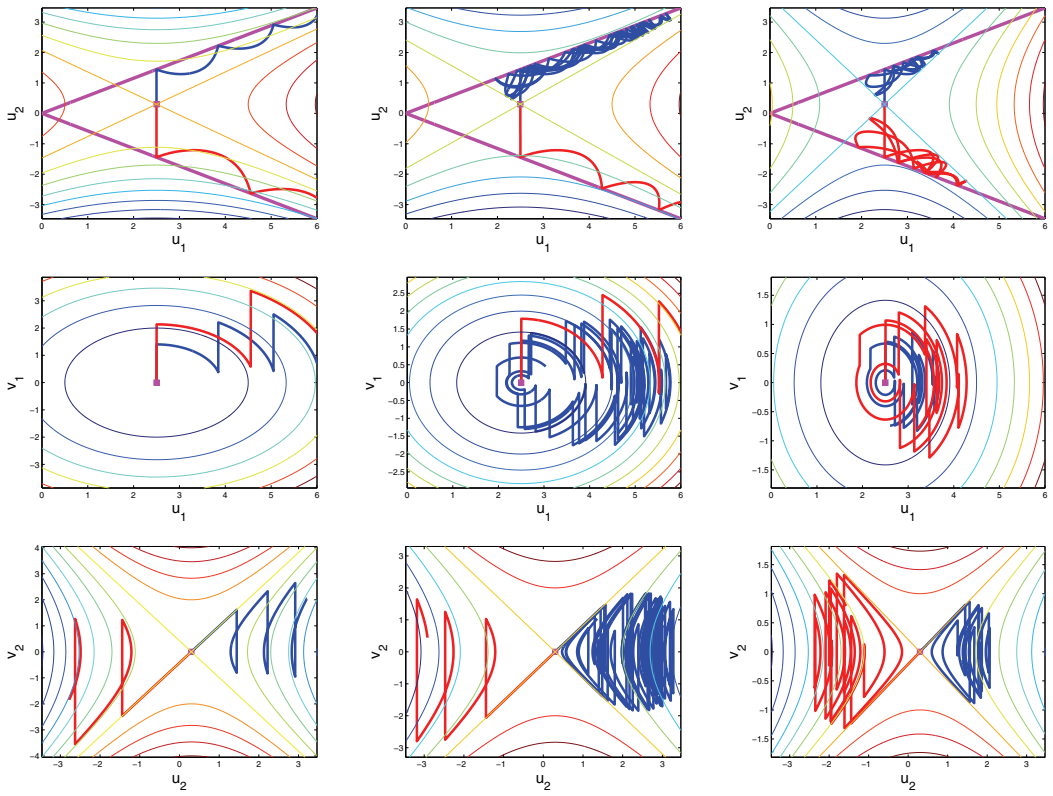

Figure 7. *SD and PCBD for the limit system* ($\varepsilon = c = 0$). *The projections of* $W^u_+(P)$ *(blue) and* $W^u_-(P)$ *(red) to the configuration space (top),* (u_1, v_1) *space (middle), and* (u_2, v_2) *space (bottom) are presented for three different* λ *values: the left, middle, and right columns have* $\lambda^2 = 2, 1.4, 0.5$, *respectively. In all figures* $\omega^2 = 1$, $u_s = (2.5, 0.3)$, $\beta = \pi/3$, $\theta = -\pi/6$, *and* $L = 6$. *The colored lines show the level curves of the quadratic potential* $V_a(u)$ *(top), the center constant* $I_1(u_1, v_1)$ *(middle), and the hyperbolic constant* $D_2(u_2, v_2)$ *(bottom). The magenta rays on the top panel indicate the impact surfaces, and the magenta squares indicate the location of the stagnation point* $(u_s, v_s = 0)$.

a necessary criterion for the creation of homoclinic tangles,[13] yet it is not sufficient, as the special case $\varepsilon = \theta = 0$ shows. Hence we call this behavior possibly complicated.

Notice that when both the upper and the lower branches exhibit SD the linear structure near the saddle point governs the motion. On the other hand, when one set has CD and the other SD we have the "open chaos" scenario in the reaction region. In particular, then the reactant/product region is strongly asymmetric. When both branches intersect we have the classical double loop homoclinic tangles. If additionally the PCBD conditions are satisfied, the chaotic motion associated with this homoclinic tangle is limited to the reaction region (and then the implications regarding scattering have yet to be explored).

Next, we show that there are some regions in the parameter space where we are able to determine that SD occurs and others where PCBD occurs. Figure 8 summarizes some of

[13]Trapping of the manifolds implies the folding back of them, but the opposite implication is not true in general: The lobes of homoclinic tangles may extend to infinity.

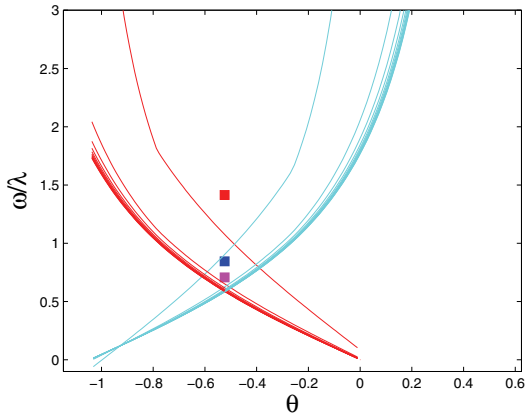

Figure 8. *The dependence of the critical values of ω/λ on θ and L. The critical values $\delta_c^{\pm}$ (see Theorems 6.2 and 6.3) for the upper (blue) and lower (red) branches of the manifolds are plotted for increasing L values. When $\omega/\lambda > \delta^{\pm}$ the upper/lower branches of P are trapped in the corner region. Here, $\beta = \pi/3$, $L = 6, 26, 46, \ldots, 206$, $u_s = (2.5, 0.3)$. The convergence at large L values is apparent. Simple behavior is expected to appear at small ω/λ, below both critical curves. The values of ω/λ for the three λ values of Figure 7 are indicated by squares (lowest, middle, upper squares correspond to left, middle, right columns of Figure 7).*

these results graphically, whereas Figures 7 and 9 demonstrate the SD and PCBD for specific parameter values.

First, we notice that independent of the saddle eigenvalues (i.e., of ω, λ), when the upper and/or lower branches of $W_{\pm}^{u,s}(P)$ do not reflect from the upper (respectively, lower) boundary ray we have SD.

Theorem 6.1 (SD I). *For sufficiently small ε, c, if $\beta + \theta \geq \pi/2$ or if $u_{1,s}\tan(\beta+\theta) > L$, there exists $h^{**}(u_{1,s}, \beta+\theta, L; \varepsilon, c) > 0$ such that for $h \in [0, h^{**})$, $W_{+}^{u,s}(\gamma_h)$ the upper branches of the stable and unstable manifolds of the Lyapunov orbit γ_h exit the corner region without intersecting each other. If $u_{1,s}\tan(\theta) < -L$, for $h < h^{**}(u_{1,s}, -\theta, L; \varepsilon, c)$ the same statement applies to the lower branches, $W_{-}^{u,s}(\gamma_h)$.*

Proof. Consider the $\varepsilon = c = 0$ case. Here the projection onto the configuration space of the extensions of $W_{+}^{u,s}(P)$ is a straight vertical segment that intersects the upper boundary of $\mathcal{A}_L$ at $(u_1, u_2) = (u_{1,s}, L)$. The corresponding phase space intersection points of $W_{+}^{u,s}(P)$ with the three-dimensional cross-section $Q = \{(u, v) | u_2 = L\}$ are $(u_1, v_1, u_2, v_2^{u,s}) = (u_{1,s}, 0, L, \pm\lambda|L - u_{2,s}|)$, so these points are well separated in phase space. Similarly, if h is not too large (see below), the traces of the stable and unstable manifolds of γ_h on Q are two planar ellipses, parallel to the (u_1, v_1) plane and separated by the finite distance $2\lambda|L - u_{2,s}|$ along the v_2 axis, so they do not intersect (this is simply the linear behavior). The restriction on h appears from the requirement that the manifolds should not hit the upper ray of the corner for any $u_2 \leqslant L$. An explicit bound on h may thus be easily found from setting $I_1 = h$ and $v_1 = 0$ in (4.7). If $\beta + \theta \geq \pi/2$, then $h < h_{obt}^{**} = \frac{\omega^2}{2}(u_{1,s})^2$ (so that γ_h does not hit the upper ray). If $u_{1,s}\tan(\beta+\theta) > L$, we require $u_1(t) < L/\tan(\beta+\theta)$ for all t, and hence $h < h_{acute}^{**} = \frac{\omega^2}{2}(\frac{L}{\tan(\beta+\theta)} - u_{1,s})^2$. The same arguments apply to the lower branches when $\theta < 0$ (replacing L by $-L$ and $(\beta+\theta)$ by θ). These results are concerned with robust properties

of trajectories within the corner region (with no impacts); hence, by the smooth dependence of trajectories within the corner region on parameters, they are clearly true for sufficiently small ε, c. ■

The second geometrical observation is that the projection of $W_+^{u,s}(\gamma_h)$ onto the configuration space lies within the Hill region of the energy level h. In particular, for $P = \gamma_0$, the Hill region boundaries are the zero potential level lines $V_a(u) = 0$ together with the corresponding boundaries of the corner region $\mathcal{A}_L$ (see below). We then notice that for sufficiently large $\frac{\omega}{\lambda}$ these zero potential level lines always intersect the corners' boundaries at $u_1 < L$, namely, that $W_+^{u,s}(\gamma_h)$ must fold back inside $\mathcal{A}_L$. We thus find the critical value of $\frac{\omega}{\lambda}$ above which the folding occurs.

Theorem 6.2 (PCBD I). *For any given geometrical parameters $(u_s, \beta+\theta, L)$ with $L > \tan(\beta+\theta)u_{1,s}$ and $\beta+\theta < \pi/2$, there exists $\delta_c^+ > \tan(\theta+\beta)$ as specified below such that for all $\frac{\omega}{\lambda} > \delta_c^+$, for sufficiently small h and (ε, c), the upper branches of the stable and unstable manifolds of the Lyapunov periodic orbit γ_h ($W_+^{u,s}(\gamma_h)$) do not exit the corner region through the product channel (i.e., with $u_2 > u_{2,s}$).*

Proof. Consider the region bounded by the corner and the upper segments of the zero level lines of the quadratic potential:

$$\mathcal{C}^+ = \mathcal{A}_L \cap \left\{(u_1,u_2)|(u_2-u_{s,2}) \geq \frac{\omega}{\lambda}|u_1-u_{s,1}|\right\}. \tag{6.1}$$

$\mathcal{C}^+$ is the Hill region for the energy level $h = 0$ for orbits of the limit system belonging to $W_+^{u,s}(\gamma_0 = P)$; since the kinetic energy must be nonnegative, orbits belonging to the energy surface $h = 0$ must satisfy for all times $V(u(t)) \leq 0$. Hence, at $\varepsilon = c = 0$, $W_+^{u,s}(P)$ is indeed trapped in $\mathcal{C}^+$. Similarly, orbits belonging to $W_+^{u,s}(\gamma_h)$ for $h > 0$ are restricted to residing in the configuration space region $\mathcal{C}_h^+$ at which $V(u(t)) \leq h$ and initially (eventually for the stable manifold) also satisfy $u_2 > u_{2,s}$.

The shape of the region $\mathcal{C}^+$ depends on the geometrical parameters. When $\tan(\theta+\beta) < \frac{\omega}{\lambda}$, the upper ray of the corner $u_2 = u_1\tan(\beta+\theta)$ intersects the upper zero potential energy level line $\{(u_1,u_2)|u_2-u_{2,s} = \frac{\omega}{\lambda}(u_1-u_{1,s}),\ u_2 > u_{2,s}\}$ at the vertex point (u_1^+, u_2^+) with

$$u_1^+ = \frac{u_{2,s} - \frac{\omega}{\lambda}u_{1,s}}{\tan(\beta+\theta) - \frac{\omega}{\lambda}} = u_{1,s} + \frac{\tan(\beta+\theta)u_{1,s} - u_{2,s}}{\frac{\omega}{\lambda} - \tan(\beta+\theta)}, \quad u_2^+ = u_1^+\tan(\beta+\theta).$$

Let $\delta_c^+ = \frac{\omega}{\lambda}$ be the eigenvalue ratio for which $L = \max(u_1^+, u_2^+)$:

$$\delta_c^+(L, u_s, \tan(\beta+\theta)) = \begin{cases} \tan(\beta+\theta) + \frac{\tan(\beta+\theta)u_{1,s}-u_{2,s}}{L-u_{1,s}} & \text{for} \quad \beta+\theta < \pi/4, \\ \tan(\beta+\theta) + \frac{\tan(\beta+\theta)u_{1,s}-u_{2,s}}{L/\tan(\beta+\theta)-u_{1,s}} & \text{for} \quad \beta+\theta > \pi/4. \end{cases} \tag{6.2}$$

Notice that for $\frac{\omega}{\lambda} > \delta_c^+$ the vertex is inside the corner region, $(\max(u_1^+, u_2^+) < L)$. Figure 8 presents the typical dependence of δ_c^+ on θ and L (blue curves).

Similarly, for sufficiently small $h > 0$, when $\frac{\omega}{\lambda} > \delta_c^+$, the right boundary of the region $\mathcal{C}_h^+$ (the upper part of the h Hill region) intersects the upper corner boundary at some finite value $(u_1^*(h), u_2^*(h) = u_1^*(h)\tan(\beta+\theta))$. Then, the shape of the upper part of the Hill region is triangular like, and orbits in its upper part have $u_1(t) < u_1^*(h) < L$. Thus, for small h,

trajectories belonging to $W_+^{u,s}(\gamma_h)$ cannot escape the corner region with $u_2 > u_{2,s}$; namely, generically, the behavior is not simple. Finally, for sufficiently small (ε, c), the restricted Hill regions are deformed into Hill regions with the same basic property: when $\frac{\omega}{\lambda} > \delta_c^+$, for sufficiently small $h \geqslant 0$, for $u_2 > u_{2,s}$, the u_1 coordinate is limited by some $u_1(t) < u_1^*(h, \varepsilon, c) < L$. ■

Note that the assumption that c is small is equivalent to requiring that the far-field terms remain small in $\mathcal{A}_L$; otherwise, these far-field terms may indeed change the shape of the Hill regions in $\mathcal{A}_L$.

A similar statement for the lower branches is the following.

Theorem 6.3 (PCBD II). *For any given geometrical parameters $(u_s, \theta < 0, L)$, there exists $\delta_c^- > -\tan\theta$ as specified below such that for all $\frac{\omega}{\lambda} > \delta_c^-$, for sufficiently small h and (ε, c), the lower branches of the stable and unstable manifolds of the Lyapunov periodic orbit γ_h ($W_-^{u,s}(\gamma_h)$) do not exit the corner region through the reactant channel (i.e., with $u_2 < u_{2,s}$).*

Proof. As in Theorem 6.2, we find the lower part of the Hill region for $h = \varepsilon = c = 0$:

$$\mathcal{C}^- = \mathcal{A} \cap \left\{ (u_1, u_2) | (u_2 - u_{s,2}) \leq \frac{\omega}{\lambda} |u_1 - u_{s,1}| \right\}. \tag{6.3}$$

If $\tan\theta > -\frac{\omega}{\lambda}$, the lower ray of the corner $u_2 = u_1 \tan\theta$ intersects the lower-right zero potential energy level line $\{(u_1, u_2) | u_2 - u_{2,s} = -\frac{\omega}{\lambda}(u_1 - u_{1,s}),\ u_2 < u_{2,s}\}$ at the point (u_1^-, u_2^-) with

$$u_1^- = \frac{u_{2,s} + \frac{\omega}{\lambda} u_{1,s}}{\tan\theta + \frac{\omega}{\lambda}} = u_{1,s} + \frac{u_{2,s} - u_{1,s}\tan\theta}{\tan\theta + \frac{\omega}{\lambda}}, \quad u_2^- = u_1^- \tan\theta.$$

Setting, for $\theta < 0$,

$$\delta_c^-(L, u_s, \tan\theta) = \begin{cases} -\tan\theta + \frac{u_{2,s} - \tan\theta u_{1,s}}{L - u_{1,s}} & \text{for} \quad -\theta < \pi/4, \\ -\tan\theta + \frac{u_{2,s} - \tan\theta u_{1,s}}{-L/\tan\theta - u_{1,s}} & \text{for} \quad -\theta > \pi/4, \end{cases} \tag{6.4}$$

we obtain that for all $\frac{\omega}{\lambda} > \delta^-(L, u_s, \tan\theta)$ the lower branches are trapped in the corner region; see Figure 8 for the typical dependence of δ_c^- on θ and L (red curves). Repeating the same arguments as for the upper branches (Theorem 6.2), the theorem is established. ■

Notice that for $\theta > 0$, for all $\frac{\omega}{\lambda}$, $u_1^- < \frac{u_{2,s}}{\tan\theta}$, namely the Hill region is always bounded. Moreover, the manifolds in this case are reflected towards the corner region. Recall that the first hit of the lower boundary of trajectories belonging to $W_-^u(P)$ is with $v_1^- = 0$, $v_2^- < 0$; hence, by (4.11), $v_1^+ < 0$. We conclude that these trajectories reflect towards the corner region, and hence the flow is not simple for $\varepsilon = c = h = 0$. Using continuity and the regular ε limit at regular reflection, we see that a similar statement applies to the small h, ε, c case. Hence, we conclude the following.

Corollary 6.4 (PCBD III). *When $\theta > 0$, the lower branches of the manifolds fold back and the flow is possibly complicated.*

Notice that when $\varepsilon > 0$, the appearance of closed level sets of the potential function (as established in the above theorems and corollary) implies that these regions also contain a minimum point of the smooth potential. Thus, we see that for large ω/λ, even though the limit system has a single saddle fixed point in the corner, the smooth system has several fixed points and some of them are stable.

Finally, Figures 7, 9, and 10 suggest that for $\theta < 0$ and sufficiently large λ SD are realized.

Conjecture 6.5 (SD II). *For any fixed geometrical parameter (u_s, θ, β, L) satisfying $-\beta < \theta < 0$, for a fixed ω and sufficiently large λ (small $\delta = \frac{\omega}{\lambda}$), for small h and sufficiently small (ε, c), both the upper and lower branches of the stable and unstable manifolds of the Lyapunov orbit γ_h ($W_{\pm}^{u,s}(\gamma_h)$) have simple behavior: They exit the corner region through the product (respectively, reactant) channel without intersecting each other in the corner domain.*

Supporting evidence. One may start by proving the claim for $h = \varepsilon = c = 0$, proving that trajectories belonging to $W_{+}^{u,s}(P)$ reflect only a finite number of regular reflections before exiting the corner region through the right side of a box of size L. Then, the claim follows by the smooth dependence of the manifolds on parameters (for sufficiently small h, c) and by the closeness of the limit system to the smooth system at regular reflections (for sufficiently small ε). Let $(u(t), v(t)) \in W_{+}^{u}(P)$ hit the upper corner ray at times t_i, $i \geq 1$, so that t_1 is its first hit. Numerical simulations show that as λ is increased the sequence of $u_1(t_i)$ is indeed monotonically increasing. Moreover, they suggest that the gaps $u_1(t_{i+1}) - u_1(t_i)$ approach a constant value: in between hits the v_1 velocity remains essentially constant since the time between reflections is roughly of order $1/\lambda^2$, whereas the changes in v_1 are on the much longer time scale $1/\omega^2$. Proving the above statements requires quite elaborate calculations of the asymptotic behavior at small δ, calculations that go beyond the scope of this manuscript.

Figures 7 and 9 demonstrate that the three different behaviors may be realized in the singular limit ($\varepsilon = 0$ in Figure 7) and in a smooth case ($\varepsilon = 0.01$ in Figure 9) when we change λ and keep all other parameters fixed. The left columns show SD in both the upper and the lower branches, the middle ones show SD in the upper branch and PCBD in the lower branch, and the right panels show PCBD in both branches. Figure 8 shows that these findings are consistent with the $\delta_c^{\pm}$ bounds for $\frac{\omega}{\lambda}$. Figure 10 shows the regularization effect that is achieved when ε is increased. Notice that even without introducing far-field potential terms, the geometrical potential level curves are reminiscent of Figure 1(b) and are similar to other PESs appearing in the chemistry literature [1, 2, 3, 4, 5, 6, 7, 8, 9].

7. Discussion.

The stable and unstable manifolds of unstable periodic orbits with energies that are slightly above the barriers' energies divide the initial isoenergetic phase space region of incoming trajectories to reacting vs. nonreacting regions [7, 8, 12]. The structure of the manifolds is called simple if these manifolds do not intersect each other and simply extend to the reactant and product channels. Then, the phase space transition state theory provides an accurate description of the transition rates from reactants to products. On the other hand, if the manifolds intersect each other or fold back into the reaction region, there is no cross-section which is crossed only once by all incoming trajectories. Then, the main assumption underlying the transition state theory fails [7, 8, 12, 18].

By introducing a geometrical model for the reaction dynamics we find conditions under which the manifolds structure is simple and conditions under which it is complicated. Three

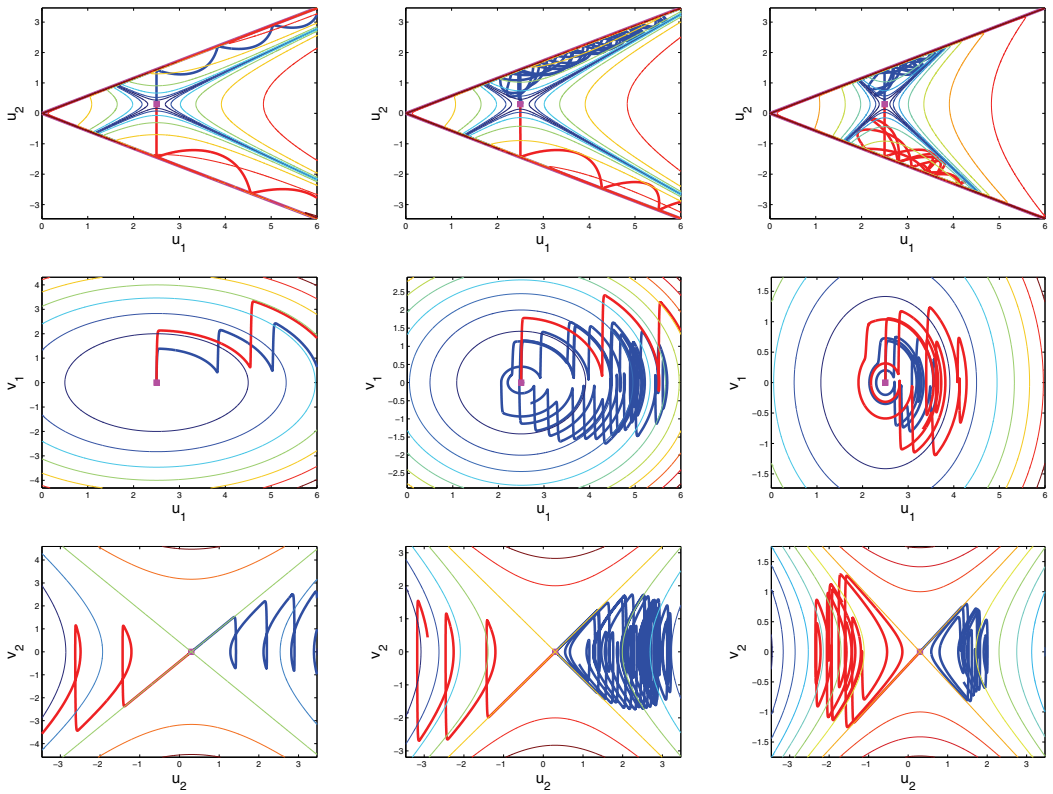

Figure 9. *SD and PCBD for the smooth system. The same parameters, initial conditions, and projections of Figure 7 are used, yet the impact flow is replaced by a smooth exponential potential along the rays ((3.3), (3.4) with $b = 10$, $\varepsilon = 0.01$). The colored lines on the top are the level curves of the smooth potential $V_a(q)+bV_b(q,\varepsilon)$.*

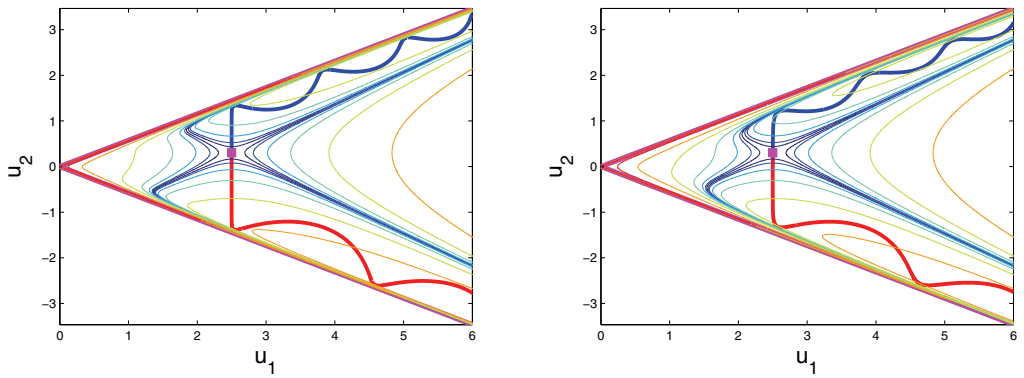

Figure 10. *SD for the smooth system: the effect of smoothing. The same parameters, initial conditions, and projection of Figure 6(a) are used with the smoothing parameter increased to $\varepsilon = 0.05$ (left) and $\varepsilon = 0.1$ (right). The smooth potential level curves still follow those of the linear potential quite closely in the region explored by $W^u_{\pm}(P)$.*

qualitative observations emerge. First, we proved that a homoclinic bifurcation occurs when the manifolds are close to being perpendicular to one of the corner rays. Then, there are intervals of energies at which stable periodic triatomic configurations emerge. In particular, in this case, transition state theory fails. Second, we found that when the projection of the unstable eigenspace to the configuration space intersects the lower corner ray in an obtuse angle (so $\theta < 0$) and the saddle-center expansion rate is much larger than the oscillation frequency, the manifolds' geometry is simple (Conjecture 6.5). Third, we established that provided the unstable eigenspace direction intersects the corner rays, the manifolds are trapped for sufficiently large oscillation frequency (Theorems 6.2 and 6.3).

We expect that similar qualitative statements may be formulated when nonlinear normal form and higher-dimensional extensions are included. Namely, we expect that conditions under which phase space transition state theory is adequate for describing the reaction for energies that are close to the saddle energy may be found by a similar methodology. More generally, while the effects of nonlinear terms in the reaction region have been suppressed here for simplicity of presentation (by taking only quadratic terms of the integrable normal form and by considering small c), we trust that the main principles that were discovered hold for the nonlinear case as well. Indeed, once the fixed point P has the saddle-center structure, its stable and unstable manifolds may be computed. With a general nonlinear smooth potential their projection to the configuration space will appear as curved lines that may or may not intersect the corner region boundary. The analysis presented here applies to the case where, in the limit system, the manifolds do hit the boundary and reflect back. Then, we expect to find similar behavior in terms of the Hill region dependence on the ratio between the oscillatory and the hyperbolic eigenvalues.

Finding the implications of the above observations for specific chemical reactions is an interesting and challenging endeavor. We believe the tools developed here may shed some light regarding the governing parameters.

Finally, we note that the analysis presented here applies to the traditional energy regime in which the behavior near the barrier is examined. The behavior for larger energies, or, equivalently, for reactions that do not have a barrier, is expected to be quite different and will be described elsewhere. Indeed, we hold that there are two distinct mechanisms that give rise to the observed sensitive dependence of the reaction rates on the energy and the initial conditions: those associated with the complicated structure of the manifolds as discussed here and those associated with the corner geometry of the nearly billiard Hamiltonian.

Appendix: The gluing map is symplectic. Let us check, for the reader's convenience, that the map $S_h : N_h^u \to N_h^s$ defined by the reflection law is a symplectic map with respect to restrictions of the main 2-form on N_h^u and N_h^s, respectively. We shall verify it for the lower wall supposing $\mu = \tan\theta$ is finite. We work in small neighborhoods of the points m_u and m_s being the intersection points for the lower branches of unstable and stable manifolds of the equilibrium P. These cross-sections belong to the 3-plane given by the relation $u_2 = \mu u_1$, and the restrictions of 2-form $dv_1 \wedge du_1 + dv_2 \wedge du_2$ to N_h^u, N_h^s are the following:

$$\hat{\omega} = d\hat{v}_1 \wedge d\hat{u}_1 + \tan\theta d\hat{v}_2 \wedge d\hat{u}_1 = (1 - \tan\theta \tfrac{\hat{v}_1}{\hat{v}_2}) d\hat{v}_1 \wedge d\hat{u}_1,$$
$$\omega = dv_1 \wedge du_1 + \tan\theta dv_2 \wedge du_1 = (1 - \tan\theta \tfrac{v_1}{v_2}) dv_1 \wedge du_1.$$

The symplecticity condition for S_h means, as is known, $S_h^*\omega = \hat{\omega}$ [43]. Using the relations $u_1 = \hat{u}_1$, $v_1 = \hat{v}_1 \cos 2\theta + \hat{v}_2 \sin 2\theta$ and the expression for $\hat{v}_2$ on N_h^u one gets

$$\begin{aligned} S_h^*\omega &= \left(1 - \tan\theta \frac{\hat{v}_1 \cos 2\theta + \hat{v}_2 \sin 2\theta}{\hat{v}_1 \sin 2\theta - \hat{v}_2 \cos 2\theta}\right) [d\hat{v}_1 \cos 2\theta + d\hat{v}_2 \sin 2\theta] \wedge d\hat{u}_1 \\ &= \left(1 - \tan\theta \frac{\hat{v}_1 \cos 2\theta + \hat{v}_2 \sin 2\theta}{\hat{v}_1 \sin 2\theta - \hat{v}_2 \cos 2\theta}\right) \left[\cos 2\theta - \sin 2\theta \frac{\hat{v}_1}{\hat{v}_2}\right] d\hat{v}_1 \wedge d\hat{u}_1 \\ &= \left(1 - \tan\theta \frac{\hat{v}_1}{\hat{v}_2}\right) d\hat{v}_1 \wedge d\hat{u}_1 = \hat{\omega}. \end{aligned}$$

Thus we get that the Poincaré map $T_h \circ S_h$ is also symplectic.

Acknowledgments. The authors thank M. Kloc and D. Tannor for their important comments and suggestions.

REFERENCES

[1] R. D. Levine, *Molecular Reaction Dynamics*, Cambridge University Press, Cambridge, UK, 2005.

[2] D. J. Tannor, *Introduction to Quantum Mechanics: A Time Dependent Perspective*, University Science Press, Sausalito, CA, 2007.

[3] N. E. Henriksen and F. Y. Hansen, *Theories of Molecular Reaction Dynamics: The Microscopic Foundation of Chemical Kinetics*, Oxford University Press, Oxford, UK, 2008.

[4] F. T. Smith, *Diabatic and adiabatic representations for atomic collision problems*, Phys. Rev., 179 (1969), pp. 111–123.

[5] P. Pechukas and E. Pollak, *Trapped trajectories at the boundary of reactivity bands in molecular collisions*, J. Chem. Phys., 67 (1977), pp. 5976–5977.

[6] E. Pollak and P. Pechukas, *Transition states, trapped trajectories, and classical bound states embedded in the continuum*, J. Chem. Phys., 69 (1978), pp. 1218–1226.

[7] E. Pollak, M. S. Child, and P. Pechukas, *Classical transition state theory: A lower bound to the reaction probability*, J. Chem. Phys., 72 (1980), pp. 1669–1678.

[8] M. J. Davis, *Phase space dynamics of bimolecular reactions and the breakdown of transition state theory*, J. Chem. Phys., 86 (1987), pp. 3978–4003.

[9] I. Burghardt and P. Gaspard, *Molecular transition state, resonances, and periodic-orbit theory*, J. Chem. Phys., 100 (1994), pp. 6395–6411.

[10] G. Haller, T. Uzer, J. Palacián, P. Yanguas, and C. Jaffé, *Transition state geometry near higher-rank saddles in phase space*, Nonlinearity, 24 (2011), pp. 527–561.

[11] G. Haller, T. Uzer, J. Palacián, P. Yanguas, and C. Jaffé, *Transition states near rank-two saddles: Correlated electron dynamics of helium*, Commun. Nonlinear Sci. Numer. Simul., 15 (2010), pp. 48–59.

[12] T. Uzer, C. Jaffé, J. Palacián, P. Yanguas, and S. Wiggins, *The geometry of reaction dynamics*, Nonlinearity, 15 (2002), pp. 957–992.

[13] M. J. Davis, *Bottlenecks to intramolecular energy transfer and the calculation of relaxation rates*, J. Chem. Phys., 83 (1985), pp. 1016–1031.

[14] M. J. Davis and R. T. Skodje, *Chemical reactions as problems in nonlinear dynamics: A review of statistical and adiabatic approximations from a phase space perspective*, in Advances in Classical Trajectory Methods, Vol. 1, JAI Press, Greenwich, CT, 1992, pp. 77–164.

[15] D. G. Truhlar, B. C. Garrett, and S. J. Klippenstein, *Current status of transition-state theory*, J. Phys. Chem., 100 (1996), pp. 12771–12800.

[16] T. Komatsuzaki and R. S. Berry, *Dynamical hierarchy in transition states: Why and how does a system climb over the mountain?*, Proc. Natl. Acad. Sci. USA, 98 (2001), pp. 7666–7671.

[17] H. Waalkens, A. Burbanks, and S. Wiggins, *A formula to compute the microcanonical volume of reactive initial conditions in transition state theory*, J. Phys. A, 38 (2005), pp. L759–L768.

[18] H. Waalkens and S. Wiggins, *Geometrical models of the phase space structures governing reaction dynamics*, Regul. Chaotic Dyn., 15 (2010), pp. 1–39.
[19] M. Inarrea, J. F. Palacian, A. I. Pascual, and J. P. Salas, *Bifurcations of dividing surfaces in chemical reactions*, J. Chem. Phys., 135 (2011), 014110.
[20] M. J. Davis and S. K. Gray, *Unimolecular reactions and phase space bottlenecks*, J. Chem. Phys., 84 (1986), pp. 5389–5411.
[21] M. Iñarrea, V. Lanchares, J. F. Palacián, A. I. Pascual, J. P. Salas, and P. Yanguas, *Rydberg hydrogen atom near a metallic surface: Stark regime and ionization dynamics*, Phys. Rev. A, 76 (2007), 052903.
[22] V. V. Kozlov and D. V. Treshchëv, *Billiards, A Genetic Introduction to the Dynamics of Systems with Impacts*, Transl. Math. Monogr. 89, American Mathematical Society, Providence, RI, 1991.
[23] V. Zharnitsky, *Invariant tori in Hamiltonian systems with impacts*, Comm. Math. Phys., 211 (2000), pp. 289–302.
[24] I. Gorelyshev and A. Neishtadt, *Jump in adiabatic invariant at a transition between modes of motion for systems with impacts*, Nonlinearity, 21 (2008), pp. 661–676.
[25] B. Gutkin, U. Smilansky, and E. Gutkin, *Hyperbolic billiards on surfaces of constant curvature*, Comm. Math. Phys., 208 (1999), pp. 65–90.
[26] D. Turaev and V. Rom-Kedar, *Islands appearing in near-ergodic flows*, Nonlinearity, 11 (1998), pp. 575–600.
[27] A. Rapoport, V. Rom-Kedar, and D. Turaev, *Approximating multi-dimensional Hamiltonian flows by billiards*, Comm. Math. Phys., 272 (2007), pp. 567–600.
[28] M. Kloc and V. Rom-Kedar, *Smooth Impact-Like Systems*, manuscript.
[29] J. C. Conley, *On the ultimate behavior of orbits with respect to an unstable critical point.* 1. *Oscillating, asymptotic, and capture orbits*, J. Differential Equations, 5 (1969), pp. 136–158.
[30] L. M. Lerman, *Hamiltonian systems with loops of a separatrix of a saddle-center*, in Methods of the Qualitative Theory of Differential Equations, Gor′kov. Gos. Univ., Gorki, 1987, pp. 89–103 (in Russian); Selecta Math. Soviet., 10 (1991), pp. 297–306 (in English).
[31] O. Yu. Kol′tsova and L. M. Lerman, *Periodic and homoclinic orbits in a two-parameter unfolding of a Hamiltonian system with a homoclinic orbit to a saddle-center*, Internat. J. Bifur. Chaos Appl. Sci. Engrg., 5 (1995), pp. 397–408.
[32] V. Rom-Kedar and D. Turaev, *Big islands in dispersing billiard-like potentials*, Phys. D, 130 (1999), pp. 187–210.
[33] A. M. Lyapunov, *The General Problem of the Stability of Motion*, Taylor & Francis, London, 1992; reprint of Internat. J. Control, 55 (1992), pp. 521–790.
[34] H. Waalkens, R. Schubert, and S. Wiggins, *Wigner's dynamical transition state theory in phase space: Classical and quantum*, Nonlinearity, 21 (2008), pp. R1–R118.
[35] O. Koltsova, L. Lerman, A. Delshams, and P. Gutiérrez, *Homoclinic orbits to invariant tori near a homoclinic orbit to center-center-saddle equilibrium*, Phys. D, 201 (2005), pp. 268–290.
[36] S. Smale, *Diffeomorphisms with many periodic points*, in Differential and Combinatorial Topology (A Symposium in Honor of Marston Morse), Princeton University Press, Princeton, NJ, 1965, pp. 63–80.
[37] L. P. Šil′nikov, *On a problem of Poincaré-Birkhoff*, Mat. Sb. (N.S.), 74 (1967), pp. 378–397.
[38] S. Newhouse, *Quasi-elliptic periodic points in conservative dynamical systems*, Amer. J. Math., 99 (1977), pp. 1061–1087.
[39] V. S. Biragov, *Bifurcations in a two-parameter family of conservative maps close to the Hénon map*, in Methods of the Qualitative Theory of Differential Equations, Gor′kov. Gos. Univ., Gorki, 1987, pp. 10–24.
[40] L. Mora and N. Romero, *Moser's invariant curves and homoclinic bifurcations*, Dynam. Systems Appl., 6 (1997), pp. 29–41.
[41] S. V. Gonchenko, L. P. Shil′nikov, and D. V. Turaev, *Dynamical phenomena in systems with structurally unstable Poincaré homoclinic orbits*, Chaos, 6 (1996), pp. 15–31.
[42] M. S. Gonchenko and S. V. Gonchenko, *On cascades of elliptic periodic points in two-dimensional symplectic maps with homoclinic tangencies*, Regul. Chaotic Dyn., 14 (2009), pp. 116–136.
[43] V. I. Arnold, *Mathematical Methods of Classical Mechanics*, Grad. Texts in Math. 60, Springer, New York, 1997.